INFORMATION TO USERS

This manuscript has been reproduced from the microfilm master. UMI films the text directly from the original or copy submitted. Thus, some thesis and dissertation copies are in typewriter face, while others may be from any type of computer printer.

The quality of this reproduction is dependent upon the quality of the copy submitted. Broken or indistinct print, colored or poor quality illustrations and photographs, print bleedthrough, substandard margins, and improper alignment can adversely affect reproduction.

In the unlikely event that the author did not send UMI a complete manuscript and there are missing pages, these will be noted. Also, if unauthorized copyright material had to be removed, a note will indicate the deletion.

Oversize materials (e.g., maps, drawings, charts) are reproduced by sectioning the original, beginning at the upper left-hand corner and continuing from left to right in equal sections with small overlaps.

Photographs included in the original manuscript have been reproduced xerographically in this copy. Higher quality 6" x 9" black and white photographic prints are available for any photographs or illustrations appearing in this copy for an additional charge. Contact UMI directly to order.

Bell & Howell Information and Learning
300 North Zeeb Road, Ann Arbor, MI 48106-1346 USA

UMI®
800-521-0600

Analytical and Experimental Studies for Space Boundary and Geometry Inverse Heat Conduction Problems

Tzu-Fang Chen

A thesis

in

The Department

of

Mechanical Engineering

Presented in Partial Fulfillment of the Requirements

For the Degree of Doctor of Philosophy

Concordia University

Montréal, Québec, Canada

April 1997

National Library
of Canada

Acquisitions and
Bibliographic Services

395 Wellington Street
Ottawa ON K1A 0N4
Canada

Bibliothèque nationale
du Canada

Acquisitions et
services bibliographiques

395, rue Wellington
Ottawa ON K1A 0N4
Canada

Your file Votre référence

Our file Notre référence

0-612-39790-4

Canada

NOTE TO USERS

Page(s) not included in the original manuscript are unavailable from the author or university. The manuscript was microfilmed as received.

ii

UMI

Abstract

Analytical and Experimental Studies for Space Boundary and Geometry Inverse Heat Conduction Problems

Tzu-Fang Chen, Ph.D.
Concordia University, 1997

Inverse Heat Conduction Problems (IHCPs) have been widely used in engineering fields in recent decades. IHCPs are not the same as direct heat conduction problems which are "well-posed". IHCPs are made more difficult since they are inherently "ill-posed"; that is, a small error perturbation will lead to a large error in the solution reconstructed. Prediction of an unknown in an IHCP is not an easy event. An IHCP also handles the desired information from measurements containing noise. A stable and accurate reliable inversion solver shall be studied.

This dissertation is split into four parts. The first part describes space boundary IHCPs, and attempts to utilize noisy measurement data to predict unknown surface temperatures or heat fluxes. A new algorithm, using a Kalman Filter to filter the measurement noise combined with an implicit time-marching finite difference scheme, solves a space boundary IHCP. In the second part, errors in reconstruction of the temperature at each boundary of a one-dimensional IHCP can be presented by a simple relation. Each relation contains an unknown coefficient, which can be determined by using one simulation through the inversion solver of a pair of specified sensor locations. This relation can then be used to estimate the other recovery errors at the boundary without using the inverse solver. In the third part, an experimental study of temperature drop between two rough surfaces is conducted. The experimental data are analyzed by utilizing an inversion solver developed in this dissertation. In the fourth part, an IHCP with a melting process using the measured temperature and heat flux at one surface is solved by a new geometry inversion solver with a heat flux limiter to reconstruct the melting front location and the temperature history inside the test domain.

Acknowledgements

I would like to express my heartfelt gratitute to my supervisers, Dr. Sui Lin and Dr. Joseph C.Y. Wang, for their valuable guidance, providing me with constant and effective support and inspiration during my Ph.D. study at Concordia University. Working for them and with them has been a very pleasant experience.

It is a pleasure to acknowledge, with many thanks, Dr. John Chao at RTZ Iron & Titanium Inc. (QIT-Fer et Titane Inc.) and Dr. Cheng-Kuei Jen at the Industrial Materials Institute, National Research Council of Canada.

I would like to dedicate this work to my parents, Mr. Cheng-Tai Chen and Mrs. Yu-Show Chen, my wife, Shih-Shan Li, my brother, Tze-Jan Chen, and all the members of my family for always standing behind me with great patience and encouragement.

I thank Mr. Alan N. Bloch, my brother in Christ in the Church in Montréal, for proof-reading this dissertation.

Contents

List of Tables

List of Figures

Chapter 1

INTRODUCTION

1.1 Background of Inverse Problems

Problems which attempt to determine effects without a precise knowledge of the causes, and "find" the unknown causes through limited observation effects, are inverse problems. Inverse problems are different from direct (forward) problems, which have enough information to determine the unknown effects. Direct problems are well-posed or correctly set, as defined by Hadamard (1923) as follows,

Definition of a well-posed problem

1. The problem is solvable and a solution exists;

2. The problem has a unique solution;

3. The solution depends continuously and stably on the given data.

A problem which is not well-posed is ill-posed. Inverse problems are ill-posed.

1.2 Classes of Inverse Heat Conduction Problems

Inverse heat conduction problems (IHCPs) may have many different classes. Here are some typical types of inverse solution processes:

1. Space Boundary IHCPs:

   The missing thermal information at the boundary of the design domain is to be found.

2. Time Backward (Retrospective) IHCPs:

   An unknown initial condition or temperature distribution in previous time is to be determined.

3. Parameter Estimation IHCPs:

   An unknown spatial and/or temporal parameter multiplier in a governing equation needs to be determined from measurement data.

4. Geometry IHCPs:

   A geometric characteristic of a heated body is to be reconstructed; for example, a phase change problem to determine the melting interface between liquid and solid phases.

All these problems are inherently ill-posed. The recovered solution may have instability phenomena due to noise in the limited observation effects. So, the numerical treatment of inverse problems must eliminate the noise from the measurement.

1.3 Examples of Direct and Inverse Problems and Historical Survey

Consider a one-dimensional heat conduction equations in a dimensionless form,

$$\frac{\partial T}{\partial t} = \frac{\partial^2 T}{\partial x^2}, \quad 0 < x < L, \quad t > 0 \tag{1.1}$$

$$T(0,t) = f_1(t), \quad x = 0, \quad t > 0 \tag{1.2}$$

$$T(L,t) = f_2(t), \quad x = L, \quad t > 0 \tag{1.3}$$

$$T(x,0) = \varphi(x), \quad 0 \leq x \leq L, \quad t = 0 \tag{1.4}$$

A direct problem with equations (1.1) to (1.4) gives the initial temperature condition $\varphi(x)$ at $t = 0$, and the Dirichlet temperature boundary conditions $f_1(t)$, $f_2(t)$ of the temperature of both sides $x = 0$ and $x = L$. There is the only one temperature solution $T(x,t)$ at any later time $t > 0$. Equations (1.1) to (1.4) constitute a well-posed problem. We use equations (1.1) to (1.4) to explain a space boundary IHCP and a time backward IHCP as follows:

1. Space Boundary IHCP: For example, if equations (1.1) to (1.4) lack boundary conditions at $x = 0$, or $x = L$, or both, use the measured temperature(s) in the interior region to reconstruct the boundary temperatures at the boundaries.

2. Time Backward IHCP: A typical inversion associated with the above heat conduction problem, equations (1.1) to (1.4), is given the temperature at time, $t = t_p > 0$, to find the temperature distribution at initial state $t = 0$.

From the examples above, we may realize that inverse problems lack adequate boundary or initial conditions. Before solving an inverse problem, we introduce the concept of the Maximum-Minimum theorem of partial differential equations.

Maximum-Minimum Theorem (Miranda, 1954):

Let region Ω be bounded and let $u(x)$ be a solution in Ω of the homogeneous equation $Du = 0$, where D is a partial differential operator of elliptic type, and suppose u is a harmonic[1] function in Ω. Then throughout the region Ω, we have

$$\min_{\partial\Omega} u < u < \max_{\partial\Omega} u \tag{1.5}$$

When the Maximum-Minimum theorem applies to elliptic-type partial differential equations (Myint-U, 1973), we may interpret this as the temperature of a conducting body with no internal heat source or sink. The maximum (or minimum) temperature will pertain to the surface boundary of the conducting body. Again, when the Maximum-Minimum theorem applies to parabolic partial differential equations (specifically heat conduction equations) (Street, 1973), we may interpret that the temperature in the domain $t > 0$ and $0 \leq x \leq L$ cannot get hotter or colder than a temperature either occurring initially or applied to the boundaries.

[1] A function is said to be harmonic in a bounded domain Ω if it satisfies the Laplace equation, and if it and its first two derivatives are continuous in Ω.

The application of the Maximum-Minimum theorem in heat conduction equations agrees with the physical phenomenon, the second law of the thermodynamics[2], and this result makes sense in the view of the well-known fact that heat flows from hot to cool. We discuss a time backward inverse problems of heat conduction equations. In general, the initial-boundary value problems for heat conduction equations cannot be solved inversely in time (Hadamard, 1923; Zachmanoglou and Thoe, 1975; Lamm, 1993; and Payne, 1993), because of the second law of thermodynamics, which states that it is impossible for a self-acting machine unaided by an external agency to move heat from one body to another at a higher temperature (Faires, 1970). Through the Maximum-Minimum theorem of heat conduction equations, we know in more detail that heat conduction is one-way in time, and also that heat conduction is an irreversible process.

Problems of recovery temperatures or heat fluxes on the surface of a conducting solid from temperature measurements made within the conducting solid are called space boundary IHCPs. In this dissertation, we are mostly interested in this type of inverse problems.

1.4 Relevant Literature

From the previous discussion, we know that direct problems have complete information in order to calculate the state of equations. However, inverse problems

[2]The second law of thermodynamics was formulated by R. Clausius in 1850.

only know part of the information, and then calculate the missing information. Direct heat conduction problems are well-posed; the solution of direct heat conduction problems have existence, uniqueness, and stability with small changes of input data (Hadamard, 1923). On the other hand, IHCPs are ill-posed in the sense that the solutions do not necessarily satisfy the conditions of existence, uniqueness, and stability with small changes of the given data. In the last three decades, IHCPs have been widely investigated by many researchers, for example, Stolz (1960), Randall (1976), Hsu *et al.* (1981), Katz and Rubinsky (1984), Beck *et al.* (1985), Kurpisz (1991), Flach and Özişik (1992), Murio (1993), and others. They have developed different techniques and numerical schemes to solve IHCPs. Stolz (1960) presented a method which has uniform initial temperature of the conducting body being quenched, and solved this IHCP by a linear superposition principle (Duhamel's principle). Stotz also pointed out that an improper selection of a time step for a given set of conditions will cause an undesirable oscillation. Frank (1963) recommended fitting the experimental data by the least squares method in solving IHCPs. A general theory for determining the temperature and heat flux at the surface of a solid was presented by Sparrow, *et al.* (1964). This theory can accommodate an arbitrarily varying initial temperature distribution throughout the solid. An integral equation presented by Deverall and Channapragada (1966) provides the recovery heat flux in IHCPs. Alifanov (1975) examined possible formulations of the problems of determining temperatures and heat fluxes at the boundary of a conducting solid from

known temperatures within the solid.

Due to the property of ill-posed problems, no unique and stable solution, it is obvious that IHCPs are sensitive to measurement errors (Hensel, 1991). In practical applications, we may deal with noisy measurement data. Also, numerically solving IHCPs will cause oscillations (Raynaud, 1986). Hills and Hensel (1986) presented a stabilizer (*i.e.* digital filter) in an inversion solver through two interior sensors, and showed the advantage of prefiltering to stabilize the results. Hills *et al.* (1986) gave the estimate of the covariance matrix of the measurement outputs, and used an adjoint formulation to solve the variance of the surface condition. When the missing information of an inverse problem is constant or a function, we may use parameter or function estimation to recover the unknown information (Beck, 1970, 1985; Hills and Hensel, 1986; Alexandrou, *et al.* 1989; Maillet, *et al.* 1991; Neto and Özişik, 1993; *etc.*). Flach and Özişik (1992) presented an optimization of a very adaptive sequential inverse heat conduction method for estimating time-dependent surface conditions of a one-dimensional region with temperature dependent properties. Rabin and Shitzer (1995) presented an analytic solution of the inverse Stefan problem in biological tissues, based on the enthalpy method; this analytical solution can also apply to non-biological materials by simply resetting the model. Sawaf and Özişik (1995) used an inverse method with an iterative procedure based on minimizing a sum of squares function to estimate linearly temperature-dependent thermal conductivity $k(T)$ and specific heat capacity $C(T)$ per unit volume for a conducting

solid.

Up to the present time, few publications on IHCPs have directly used measurement information and simultaneously imported it to the numerical scheme. Scarpa and Milano (1995) used a Kalman Smoothing Technique in dealing with the transient state boundary heat flux, to smooth and reconstruct surface heat flux with explicit forward or Crank-Nicolson difference schemes. Some useful textbooks by Beck (1985), Hensel (1991), Murio (1993), and Alifanov (1994) have many examples of how to handle the measurement error of inverse problems. Those books are good reviews in the inverse engineering field.

Based on the above literature survey, there does not exist an easy on-line and real-time monitoring inverse solver for space boundary inverse heat conduction problems. Chen *et al.* (1996) propose a new on-line real-time filtering method for eliminating the noise directly from the measurement data. Then these "post-clean" data are utilized for the inverse solver to recover the boundary temperature and heat fluxes on the surface.

It is also noted that all solvers mentioned above are based on multiple spatial position measurement sensors to recover their results. In Chapter 7, we consider a one-dimensional inverse Stefan problem by measuring one-sided transient temperature and heat flux to recover the temperature history and the melting front position inside the body. A semi-explicit time marching finite difference scheme (Chen *et al.*, 1997b) is developed to recover the unknown temperature history and the melting

front, with only one-sided temperature and heat flux boundary conditions. In order to reduce errors caused by instability, here we also introduce a heat flux limiter to damp the numerical oscillations. Numerical solutions with and without the heat flux limiter are presented in comparison to an exact solution through N-Eicosene paraffin wax.

1.5 Objectives of the Thesis

Inverse problems have many applications, for example, heat transfer processes associated with re-entry of space vehicles, temperature prediction of a combustion chamber, determination of material thermophysical properties through temperature functions, nondestructive evaluation (NDE) of material, determination of contact resistance between two rough surfaces, and others. The objectives of this dissertation are:

1. to find a new approach to solving IHCPs through a real-time filter to handle noisy measurement data.

2. to develop an inversion solver insensitive to measurement errors.

3. to find an inversion solver which can reduce instability phenomena directly from noise oscillation of the measurement.

4. to formulate a simple error-sensor-location prediction equation. This equation can predict the recovery surface temperature error due to different sensor

locations inside the conducting solid.

5. to compare numerical recovering results with experimental data.

6. to show the adaptation of an inversion solver to a real engineering problem.

7. to determine the temperature difference due to contact resistance between two rough surfaces.

8. to apply one-sided boundary conditions to predict the interior temperature profile and melting front.

1.6 Thesis Overview

The dissertation is organized in eight chapters as follows:

Chapter 1, the background and relevant literature on IHCPs.

Chapter 2, an inversion model for IHCPs.

Chapter 3, a Kalman Filter and its recovery solutions in IHCPs.

Chapter 4, determination of boundary temperature errors in one-dimensional IHCPs.

Chapter 5, the experimental work.

Chapter 6, reconstructing results from experimental measurement.

Chapter 7, a finite difference inversion scheme with a heat flux limiter to solve a one-dimensional inverse Stefan problem.

Chapter 8, conclusions and future work.

Chapter 2

Inversion Model for Inverse Heat Conduction Problems

This chapter considers the inversion model as follows:

- The locations of the two interior temperature measurements are at positions $x = \chi_L$ and $x = \chi_M$, as shown in Figure 2.1.
- Temperatures and heat fluxes can be reconstructed on both sides of the boundaries at $x = \chi_o = 0$ and $x = \chi_N$.

This numerical scheme (Chen, *et al.*, 1996) will be stated in section 2.2.

2.1 Exact Solutions used for Testing IHCPs

To investigate the inversion error of the numerical solver, two exact heat conduction solutions will be used, a semi-infinite solid (exact solution I) and a finite thickness

wall (exact solution II), presented in the following sections.

2.1.1 Exact Solution I: A semi-infinite solid

The dimensionless system of equations for the semi-infinite solid containing a time-dependent Dirichlet boundary condition at the boundary $x = \chi_o = 0$ is formulated as follows:

$$\frac{\partial T}{\partial t} = \frac{\partial^2 T}{\partial x^2} \tag{2.1}$$

$$T(x,0) = 0 \tag{2.2}$$

$$T(0,t) = f(t) \tag{2.3}$$

$$T(\infty,t) = 0 \tag{2.4}$$

The exact solution of the problem (Carslaw and Jaeger, 1959) is:

$$T(x,t) = \frac{2}{\sqrt{\pi}} \int_{\frac{x}{2\sqrt{t}}}^{\infty} f(t - \frac{x^2}{4\mu^2}) e^{-\mu^2} d\mu \tag{2.5}$$

The semi-infinite heat conduction equation with exact solution is used for investigating the recovering results of the IHCP. In this exact model, we address the problem of the conducting solid with two interior sensors. The temperatures of the sensor measurements at point $x = \chi_L$ (left hand sensor) and at point $x = \chi_M$ (right

hand sensor) are known (Figure 2.1). Take the temperature data at the measurement sensor positions, $x = \chi_L$ and $x = \chi_M$, from equation (2.5) of the exact solution, as the input of the time marching finite difference scheme. Then, the numerical recovery results are compared with the exact solutions which are at the left boundary ($x = \chi_o = 0$) and at the right computational domain boundary ($x = \chi_N = 1$) of the semi-infinite solid.

2.1.2 Exact Solution II: A finite thickness wall

The dimensionless system of equations for a wall having finite thickness l, containing Neumann boundary conditions at both sides, *i.e.* a zero heat flux at $x = \chi_o = 0$ and a time-dependent heat flux at $x = \chi_N = l$, is described as follows:

$$\frac{\partial T}{\partial t} = \frac{\partial^2 T}{\partial x^2} \tag{2.6}$$

$$T(x,0) = 0 \tag{2.7}$$

$$\frac{\partial T(0,t)}{\partial x} = 0 \tag{2.8}$$

$$\frac{\partial T(l,t)}{\partial x} = q(t) \tag{2.9}$$

The exact solution of the problem (Hills, *et al.*, 1986) is:

$$T(x,t) = \frac{3x^2-l^2}{6l}q(t) - q(t)\frac{2}{l}\sum_{k=1}^{\infty}\frac{(-1)^k}{\mu_k{}^2}cos(\mu_k x) + \frac{1}{l}\int_0^t q(\tau)d\tau$$
$$+\frac{2}{l}\sum_{k=1}^{\infty}(-1)^k\int_0^t q(\tau)e^{-\mu_k{}^2(t-\tau)}d\tau cos(\mu_k x) \tag{2.10}$$

where

$$\mu_k = \frac{k\pi}{l} \tag{2.11}$$

The heat conduction equation with exact solution is used to compare the output surface heat fluxes of the IHCP simulation results. With the two fixed sensor locations, the temperatures of the sensor measurements at point $x = \chi_L$ (one-third of the length of the test specimen) and at point $x = \chi_M$ (two-thirds of the length of the test specimen) are known (see Figure 2.1). The heat fluxes at the left hand boundary ($x = 0$) and at the right hand boundary ($x = \chi_N = 1.2$) can be determined by the numerical scheme of the IHCP.

2.2 Numerical scheme of the IHCP

The time-marching finite difference scheme can be divided into two classes: the explicit scheme, which involves only one unknown grid point at the advanced time level $(n+1)\Delta t$, and the implicit scheme, which involves more than one unknown grid point at the advanced time level $(n+1)\Delta t$.

An unconditionally stable fully implicit finite difference scheme of dimensionless heat conduction equations (2.1) or (2.6) can be written in the form:

$$U\underline{T}^{n+1} = \underline{T}^{n} \tag{2.12}$$

Where U is a matrix with forward and backward shift operators S_+ and S_-. For example, the finite difference scheme equation (2.12) is

$$-\lambda T_{i+1}^{n+1} + (1+2\lambda)T_i^{n+1} - \lambda T_{i-1}^{n+1} = T_i^n \tag{2.13}$$

where λ is equal to $\frac{\Delta t}{(\Delta x)^2}$. By using shift operators S_+ and S_-, equation (2.13) becomes

$$-\lambda S_+ T_i^{n+1} + (1+2\lambda)T_i^{n+1} - \lambda S_- T_i^{n+1} = T_i^n \tag{2.14}$$

or

$$(-\lambda S_+ + (1+2\lambda) - \lambda S_-)T_i^{n+1} = T_i^n \tag{2.15}$$

where T_i^n are the elements of matrix $\underline{T}^n$.

Applying the left hand boundary heat flux q_o^{n+1} at the $(n+1)\Delta t$ time level to the finite difference scheme, equation (2.13), gives

$$(1+\lambda)\,T_o^{n+1} - \lambda T_1^{n+1} + \lambda \Delta x q_o^{n+1} = T_o^n \tag{2.16}$$

Similarly, applying the right hand boundary heat flux q_N^{n+1} at the $(n+1)\Delta t$ time level to the finite difference scheme yields

$$(1+\lambda)\,T_N^{n+1} - \lambda T_{N-1}^{n+1} - \lambda \Delta x q_N^{n+1} = T_N^n \tag{2.17}$$

The corresponding temperatures of the two sensors at points $x = \chi_L$ and $x = \chi_M$ (as shown in Figure 2.1) at the $(n+1)\Delta t$ time level, T_L^{n+1} and T_M^{n+1}, are known. The unknown heat fluxes at both boundaries, q_o^{n+1} and q_N^{n+1}, can be substituted into the positions of the elements T_L^{n+1} and T_M^{n+1}, respectively, in matrix $\underline{T}^{n+1}$ of equation (2.12). The two unknown boundary heat flux coefficients, $+\lambda\Delta x$ for q_o^{n+1} and $-\lambda\Delta x$ for q_N^{n+1}, can then be substituted into the corresponding element positions in the U matrix of equation (2.12). Then the two known sensor measured temperatures, T_L^{n+1} and T_M^{n+1}, can be put into the positions of elements T_L^n and T_M^n, respectively, in matrix $\underline{T}^n$ of equation (2.12).

Matrix U of equation (2.12) is expressed as,

$$U = \begin{bmatrix} 1+\lambda & -\lambda & 0 & \cdots & 0 & 0 & \lambda\Delta x & 0 & 0 & \cdots & 0 & & & 0 \\ & & & & \cdot & \cdot & \cdot & & & & & & & \\ & & & & -\lambda & 1+2\lambda & 0 & & & & & & & \\ & & & & & -\lambda & 0 & -\lambda & & & & & & \\ & & & & & & 0 & 1+2\lambda & -\lambda & & & & & \\ & & & & & & & \cdot & \cdot & \cdot & & & & \\ & & & & & & & & -\lambda & 1+2\lambda & 0 & & & \\ & & & & & & & & & -\lambda & 0 & -\lambda & & \\ & & & & & & \cdot & & & & 0 & 1+2\lambda & -\lambda & \\ & & & & & & & & & & \cdot & \cdot & \cdot & \cdot \\ 0 & & & & & & 0 & & & \cdots & -\lambda\Delta x & \cdots & -\lambda & 1+\lambda \end{bmatrix} \tag{2.18}$$

The unknown matrix $\underline{T}^{n+1}$ of equation (2.12) can be written as:

$$\underline{T}^{n+1} = \begin{bmatrix} T_o^{n+1} \\ . \\ T_{L-1}^{n+1} \\ q_o^{n+1} \\ T_{L+1}^{n+1} \\ . \\ T_{M-1}^{n+1} \\ q_N^{n+1} \\ T_{M+1}^{n+1} \\ . \\ T_N^{n+1} \end{bmatrix} \tag{2.19}$$

Matrix $\underline{T}^n$ of equation (2.12) has the form:

$$\underline{T}^n = \begin{bmatrix} T_o^n \\ . \\ T_{L-1}^n + \lambda T_L^{n+1} \\ T_L^n - (2\lambda+1) T_L^{n+1} \\ T_{L+1}^n + \lambda T_L^n \\ . \\ T_{M-1}^n + \lambda T_M^{n+1} \\ T_M^n - (2\lambda+1) T_M^{n+1} \\ T_{M+1}^n + \lambda T_M^{n+1} \\ . \\ T_N^n \end{bmatrix} \tag{2.20}$$

Then, the unknown matrix $\underline{T}^{n+1}$ (including boundary temperatures and boundary heat fluxes at both sides) can be solved by this implicit time marching scheme.

2.3 Stability Analysis

For a time-marching scheme, a proper time step size must be chosen to account for the numerical accuracy and stability. A weighted Euler scheme is considered, so that equation (2.1) or (2.6) can be rewritten as

$$\frac{T_i^{n+1} - T_i^n}{\triangle t} = \frac{\theta}{\triangle x^2}\delta^2{}_x T_i^{n+1} + \frac{(1-\theta)}{\triangle x^2}\delta^2{}_x T_i^n \tag{2.21}$$

where

$$\delta_x{}^2 T_i^{n+1} \equiv T_{i-1}^{n+1} - 2T_i^{n+1} + T_{i+1}^{n+1} \tag{2.22}$$

The temperature function is expanded in a Fourier series, such that

$$T(x,t) = \sum_{k=-(N-1)}^{N-1} \Lambda_k(t) e^{i\mu_k x} \tag{2.23}$$

where the discrete numerical approximation has the coefficients $\Lambda_k(t)$.

The definition of μ_k in equation (2.23) is shown in equation (2.11).

The amplification factor is defined by:

$$g = \frac{\Lambda_k(t^{n+1})}{\Lambda_k(t^n)} \tag{2.24}$$

which can be obtained by substituting equation (2.23) into equation (2.21) as follows:

$$g = \frac{-1 + 4\lambda(1-\theta)sin^2(\mu_k \frac{\triangle x}{2})}{1 + 4\lambda\theta sin^2(\mu_k \frac{\triangle x}{2})} \tag{2.25}$$

The numerical stability requires that $|g| \leq 1$. Then the stability condition is:

$$\lambda(1-2\theta) \leq 0.5 \tag{2.26}$$

The constraint equation (2.26) implies that the explicit scheme (*i.e.* $\theta = 0$) has a stability bound of $\lambda \leq 0.5$. However, if the scheme has the value of $\theta \geq 0.5$, it is unconditionally stable. The finite difference scheme of equation (2.12) with $\theta = 1$ is a fully implicit and unconditionally stable scheme.

2.4 Numerical Experiments

Numerical experiments are divided into two parts as follows:

(1) Error percentage in Dirichlet boundary conditions

We consider the Dirichlet boundary temperature function $f(t)$ in equation (2.3) as a linear function

$$f(t) = 50t \tag{2.27}$$

Use equation (2.27) as the recovery temperature boundary at left hand boundary $x = \chi_o = 0$, and consider the locations of the two temperature sensors at $x = 0.2$ and $x = 0.4$ in the dimensionless scale for the numerical simulation. The values of the temperature errors at the left hand boundary ($x = \chi_o = 0$) and at the right hand boundary of the computational domain ($x = \chi_N = 1$) are determined to be 0.374% and 2.62% respectively.

(2) Recovery of surface heat fluxes

To test the stability of the numerical scheme, the exact solution of the finite thickness wall problem, equation (2.10), with a nonlinear step function of heat flux $q(t)$ in equation (2.9) at the right hand boundary $x = \chi_N = 1.2$ is used. If this step function can be recovered well, then certainly other kinds of continuous functions of the heat flux could be recovered better. For the simulation, the temperatures of the sensor positions at $x = \chi_L = 0.4$ and $x = \chi_M = 0.8$ are taken from the exact solution, equation (2.10). With the mesh size $\Delta x = 0.1, \Delta t = 0.1$ and the mesh size $\Delta x = 0.05, \Delta t = 0.05$, the surface heat fluxes at $x = 0$ and $x = \chi_N = 1.2$ are calculated as shown in Figures 2.2 and 2.3, respectively. Both of the recovered heat fluxes are close to the exact heat fluxes.

2.5 Summary

The implicit time marching finite difference scheme in this chapter for recovering the time history of boundary temperature and heat fluxes is in good agreement for inversion.

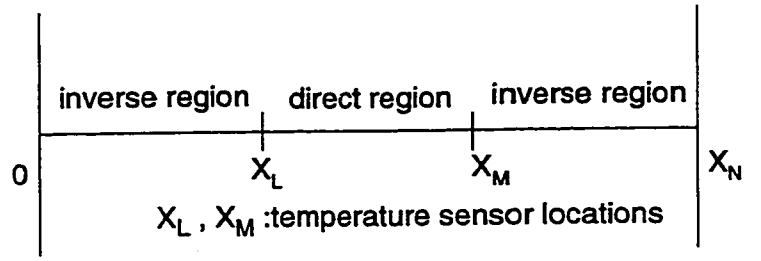

Unknown conditions:
$Q(0,t) = ?$, $Q(X_N, t)=?$
$T(0,t) = ?$, $T(X_N, t)=?$

Known conditions:
$T(X_L,t) =$ known
$T(X_M,t) =$ known

Figure 2.1: One-dimensional inverse heat conduction problem

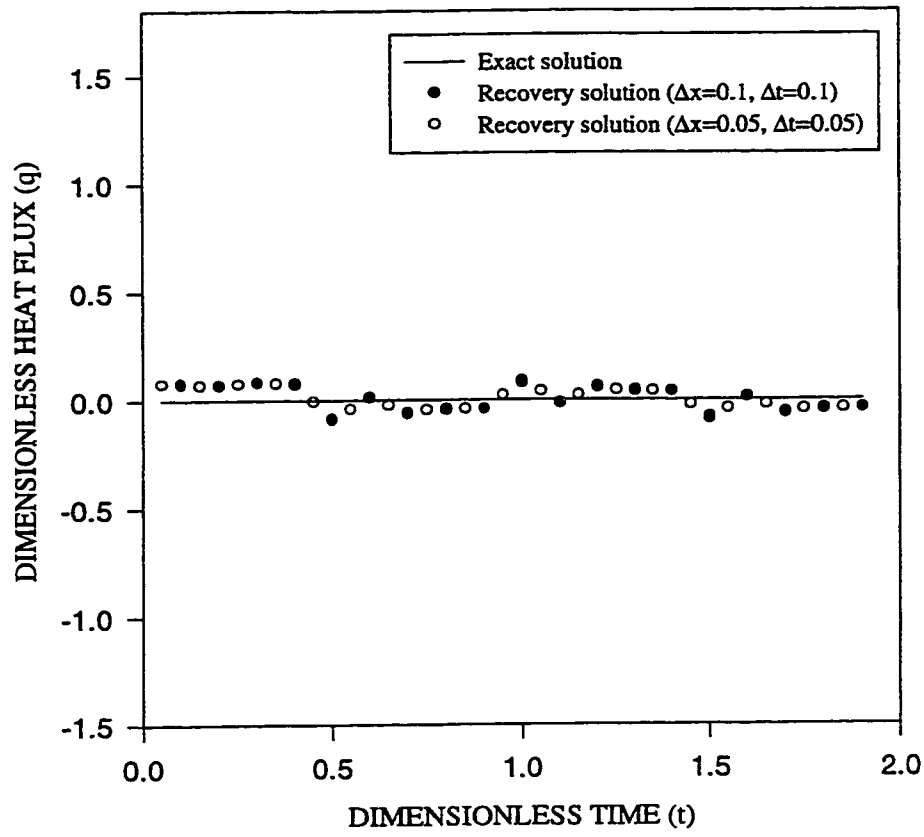

Figure 2.2: Comparison of the exact heat flux and recovered heat flux at the boundary, $x = 0$

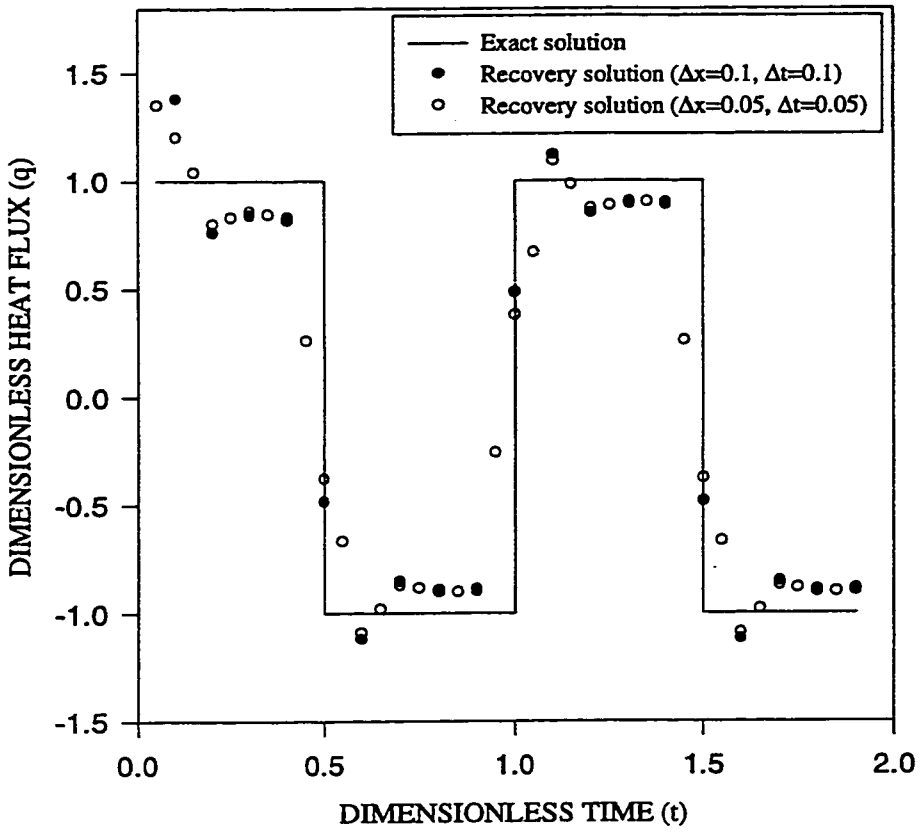

Figure 2.3: Comparison of the exact heat flux and recovered heat flux at the boundary, $x = l = 1.2$

Chapter 3

Kalman Filter and Its Recovery Results

3.1 Background

In order to obtain an accurate recovery boundary temperature or heat flux, it is necessary to determine and to reduce the errors caused by the temperature measurements. A Kalman Filter is a good method for handling the random noise directly from the real-time measurement. Because a Kalman Filter is a real-time filter, the inversion solver can combine a Kalman Filter to invert a real-time IHCP. In this chapter, a model of IHCPs is formulated by imposing random noise on an exact solution of a one-dimensional heat conduction problem. A "real-time" Kalman Filter (Sorenson, 1966) for stabilizing noisy measurement data is used with a finite difference scheme to recover the temperature or heat flux on the surface of the conducting body.

3.2 Kalman Filter for Measured Temperature Values

Random noise exists in any experimental measurement, and should be eliminated for data analysis. There are many kinds of techniques which can estimate data from experiments, such as Least Square Estimator, Maximum Likelihood Estimator, Kalman Filter, *etc.* The Kalman Filter is a real-time estimator, which needs only the one previous data point at time $n\Delta t$ to predict the following data point at time $(n+1)\Delta t$. In this chapter, the Kalman Filter is used to estimate the measurement temperature data from the sensor output. The following is the Kalman Filter method specifically used for the present inverse problem.

For temperature measurement, it is assumed that at each time t^{n+1}, there are measurement values, $\underline{y}^{n+1}$, available, and that the measured values are linearly related to the state vector (the true temperature matrix, $\underline{z}^{n+1}$), and the additive white noise, $\underline{v}^{n+1}$. Then

$$\underline{y}^{n+1} = \underline{C}^{n+1}\underline{z}^{n+1} + \underline{v}^{n+1} \tag{3.1}$$

Where $\underline{C}^{n+1}$ is a known observation matrix. In the present paper, $\underline{C}^{n+1}$ is presented by:

$$\underline{C}^{n+1} = \begin{bmatrix} 1 & 0 \end{bmatrix} \tag{3.2}$$

The temperature variation at a fixed position may be represented by a second-order time derivative, and a state vector introduced as follows:

$$\frac{d^2T}{dt^2} = a(t) \tag{3.3}$$

$$\underline{z}(t) = \begin{bmatrix} z_1(t) \\ z_2(t) \end{bmatrix} \tag{3.4}$$

where

$$z_1(t) = T(t) \tag{3.5}$$

$$z_2(t) = \frac{dT(t)}{dt} \tag{3.6}$$

Equation (3.3) can then be written in the form:

$$\frac{d\underline{z}(t)}{dt} = \begin{bmatrix} 0 & 1 \\ 0 & 0 \end{bmatrix} \underline{z}(t) + \begin{bmatrix} 0 \\ a(t) \end{bmatrix} \tag{3.7}$$

The solution of $\underline{z}(t)$ is obtained by:

$$\underline{z}(t) = \underline{A}(t,\tau)\ \underline{z}(\tau) + a(t) \begin{bmatrix} \frac{(t-\tau)^2}{2} \\ (t-\tau) \end{bmatrix} \tag{3.8}$$

Where, $\underline{A}$ is the state transition matrix as follows:

$$\underline{A} = \begin{bmatrix} 1 & t-\tau \\ 0 & 1 \end{bmatrix} \tag{3.9}$$

Equation (3.8) can be presented by the following two equations:

$$z_1(t) = z_1(\tau) + (t-\tau)z_2(\tau) + \frac{a(t)}{2}(t-\tau)^2 \tag{3.10}$$

$$z_2(t) = z_2(\tau) + a(t)(t-\tau) \tag{3.11}$$

For numerical calculation, let

$$t = (n+1)\Delta t,\ \tau = n\Delta t \tag{3.12}$$

Then equation (3.8) becomes

$$\underline{z}^{n+1} = \begin{bmatrix} 1 & \Delta t \\ 0 & 1 \end{bmatrix} \underline{z}^n + a(t) \begin{bmatrix} \frac{(\Delta t)^2}{2} \\ (\Delta t) \end{bmatrix} \tag{3.13}$$

Equation (3.13) is the difference equation representing the matrix system of the true temperature and the rate of change of the temperature.

The Kalman Filter contains the following parts (Sorenson, 1966):

(i) Compute Kalman gain $\underline{G}^{n+1}$:

$$\underline{G}^{n+1} = \underline{P_1}^{n+1}\underline{C}^{n+1^T}[\,\underline{C}^{n+1}\underline{P_1}^{n+1}\underline{C}^{n+1^T} + \underline{R}^{n+1}]^{-1} \tag{3.14}$$

where $\underline{R}^{n+1}$ is related to the expected value

$$\underline{R}^{n+1} = E\left[\underline{v}^{n+1},\ \underline{v}^{n+1^T}\right] \tag{3.15}$$

and

$$\underline{P_1}^{n+1} = \underline{A}^{n+1} \underline{P}^n \ \underline{A}^{n+1T} \tag{3.16}$$

(ii) Compute error covariance matrix $\underline{P}^{n+1}$:

$$\underline{P}^{n+1} = \underline{P_1}^{n+1} - \underline{G}^{n+1} \ \underline{C}^{n+1} \underline{P_1}^{n+1} \tag{3.17}$$

(iii) Update estimate with measurement y^{n+1} (the filtering results of the Kalman Filter):

$$\underline{\hat{z}}^{n+1} = \underline{A}^{n+1} \underline{\hat{z}}^n + \ \underline{G}^{n+1} [\underline{y}^{n+1} - \underline{C}^{n+1} \ \underline{A}^{n+1} \underline{\hat{z}}^n] \tag{3.18}$$

3.3 Numerical Experiments

The calculation procedures combining the Kalman Filter and the time marching implicit finite difference scheme are as follows (Chen *et al.*, 1996):

- Step 1: Smoothing the noisy data of the temperature sensor output from the measurement points at $x = \chi_L$ and $x = \chi_M$ by the Kalman Filter at the $(n+1)\Delta t$ time level.

- Step 2: Recovering the surface temperature or heat flux at the $(n+1)\Delta t$ time level by using the inversion time marching implicit finite difference solver with

the temperature filtering data treated in step 1.

We consider the Dirichlet boundary temperature function $f(t)$ at $x = 0$ in equation (2.3) as a quadratic function

$$f(t) = 0.21t^2 \tag{3.19}$$

The method of the Kalman Filter, described in equations (3.1)-(3.18), is used to eliminate the random noise which is generated by adding random noise of $\pm 12.5\%$ of the data obtained from the exact solution. Figures 3.1 and 3.3 show the exact solutions with noisy data at positions $x = \chi_L$ and $x = \chi_M$ respectively. Figures 3.2 and 3.4 show the results of the temperature time histories obtained by the Kalman Filter, which are very close to the exact solutions with maximum errors of 3.6% and 3.65%, at positions $x = \chi_L$ and $x = \chi_M$ respectively. Figure 3.5 shows three temperature results with and without Kalman Filter simulation solution (dot points and plus points respectively), and the exact solution (full line) at the dimensionless time $t = 100$ (the maximum error percentages are 1.9% and 20.8% respectively). Figures 3.6 and 3.7 show the three results of the time history of the recovery heat fluxes on the left and right hand boundaries respectively: the exact solution (full line), the simulation with Kalman Filter (dot points), and the simulation without Kalman Filter (plus points). It can be seen that the solutions of the noisy data simulation without using the Kalman Filter oscillate further away from the exact solution, and may diverge away from the exact solution.

3.4 Summary

The Kalman Filter used in this chapter is a real-time prefilter. It smooths the temperature noise in a real-time way. The smoothed data are used in the inversion solver to prevent the instability caused by the random noise of the measurement temperature inside the conducting solid.

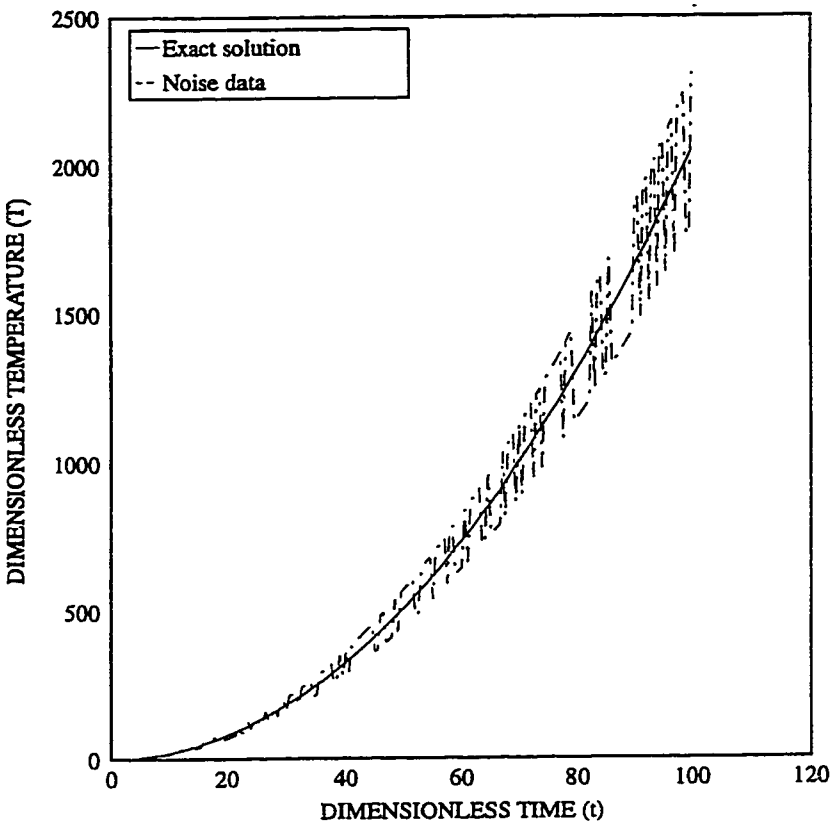

Figure 3.1: Comparison of the exact temperature and noisy data at point L

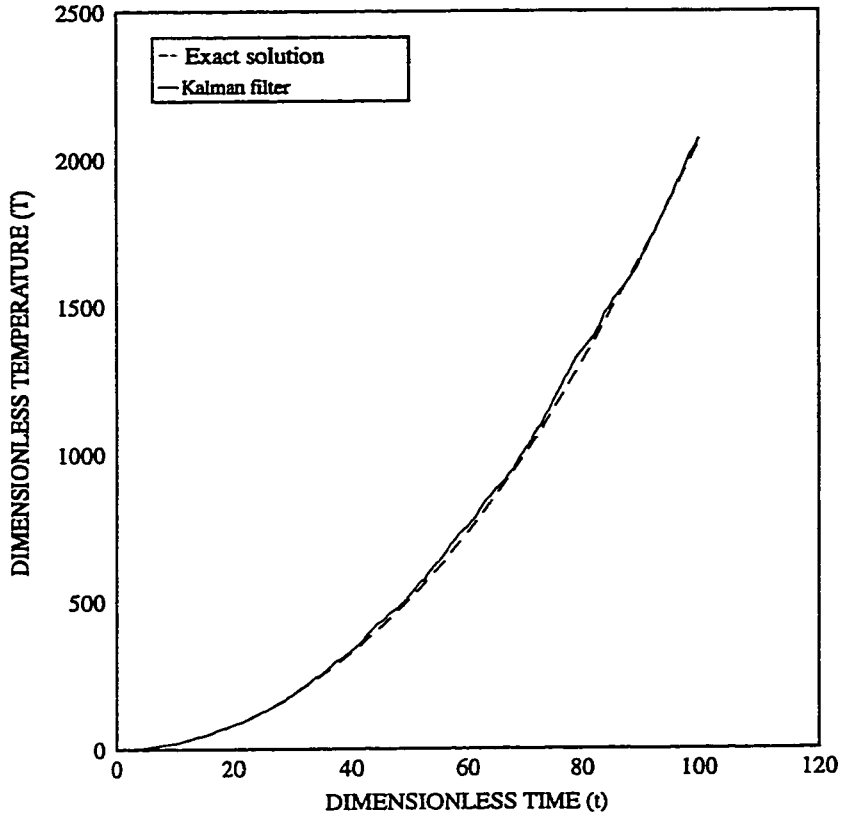

Figure 3.2: Comparison of the exact temperature and Kalman Filtering result at point L

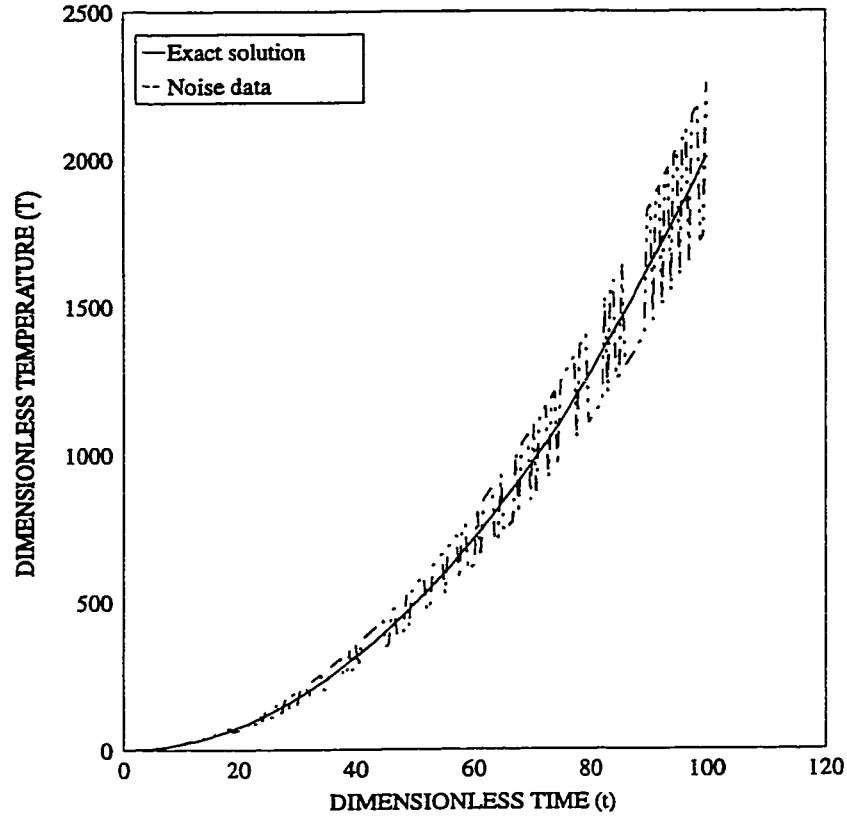

Figure 3.3: Comparison of the exact temperature and noisy data st point M

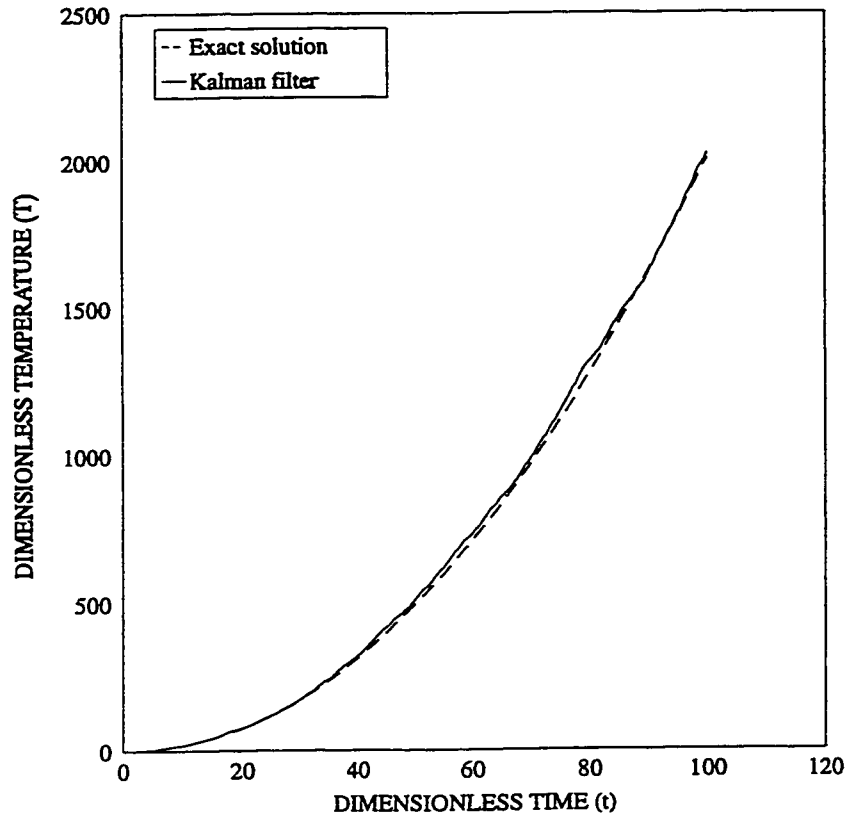

Figure 3.4: Comparison of the exact temperature and Kalman Filtering result at point M

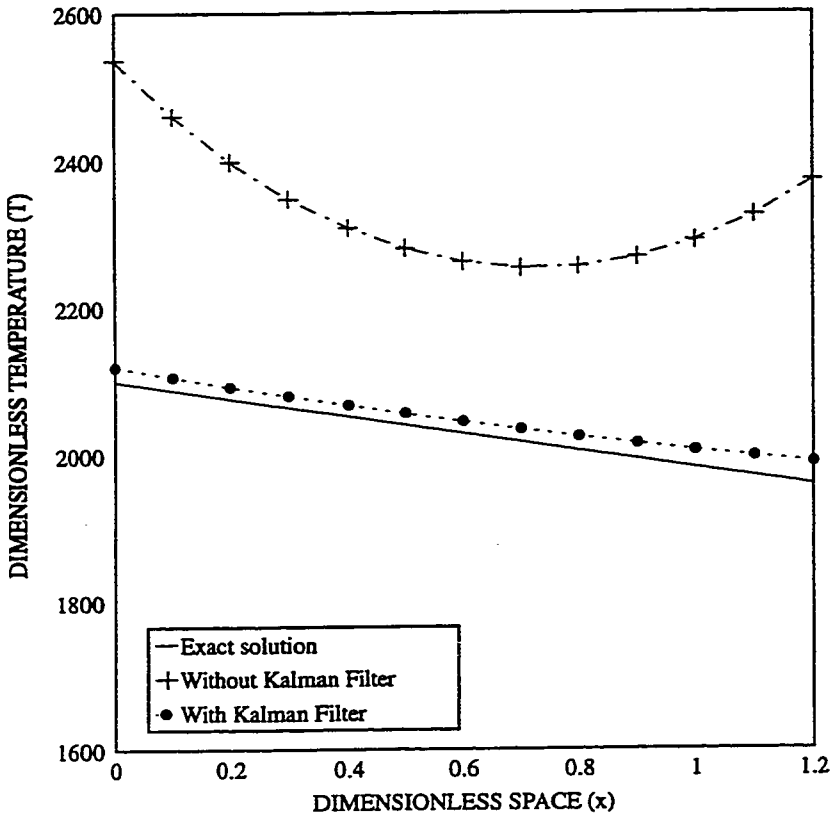

Figure 3.5: Comparison of exact, with and without Kalman Filtering recovering results at dimensionless time $t = 100$

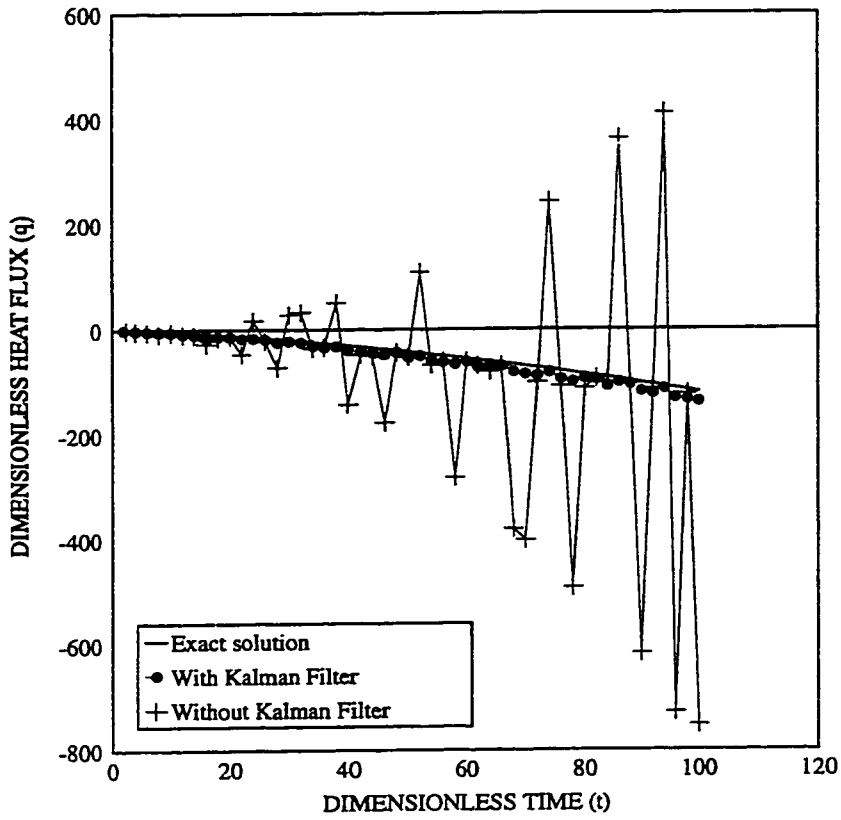

Figure 3.6: Comparison of three time histories of the recovery heat flux at the left hand boundary $x = 0$

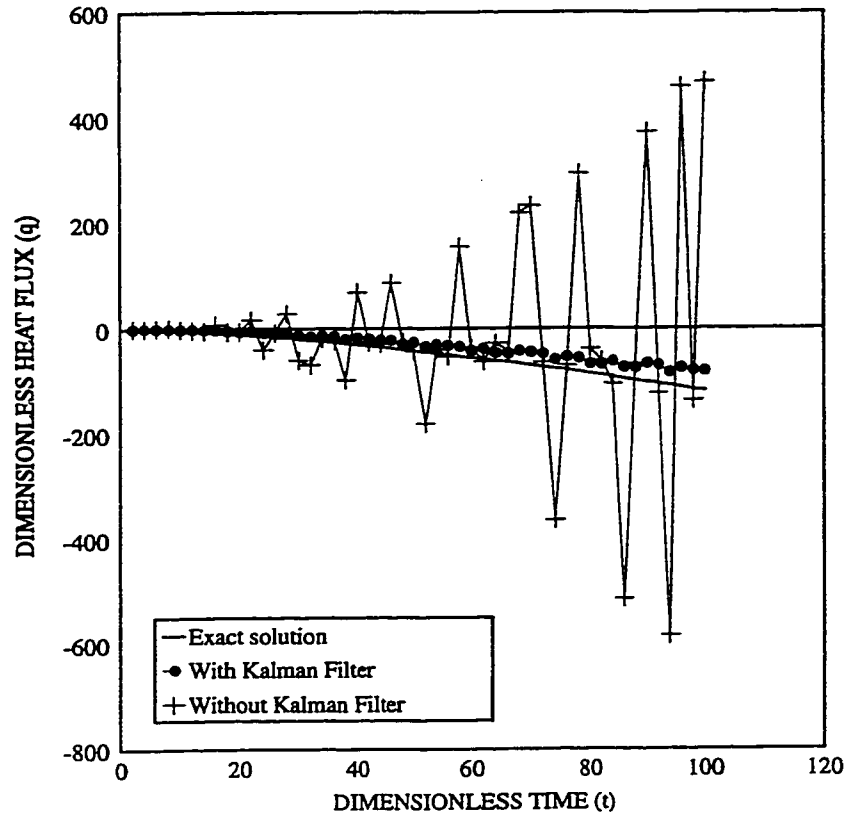

Figure 3.7: Comparison of three time histories of the recovery heat flux at the right hand boundary $x = 1.2$

Chapter 4

Determination of Boundary Temperature Recovery Errors in One-dimensional Inverse Heat Conduction Problems

4.1 Introduction

Errors in temperature recovery at boundaries caused by variation of the locations of two temperature sensors in a one-dimensional IHCP have been investigated by using a time marching implicit finite difference scheme. Numerical simulation results of selected functions indicate that errors of the reconstruction temperature at each boundary may be expressed by a simple relation (Chen *et al.*, 1997a). Each relation contains an unknown coefficient, which can be determined by using one numerical simulation through the inversion solver of a pair of specified sensor locations. This

relation can then be used for estimating the other recovery errors at the boundary without using the inversion solver.

In order to have a reliable estimate of the temperature on the surface, errors caused by the locations of interior temperature sensors shall be investigated. This chapter considers a one-dimensional IHCP in dimensionless form, which is solved by using the time marching implicit finite difference scheme shown in Section 2.2, and investigates the errors caused by the variation of two interior sensor locations. Simple error relations have been established from the numerical results of selected boundary functions for estimating the errors of reconstruction temperatures at the both side boundaries .

4.2 An Exact Solution used for Error Prediction of IHCP

In this section, we use exact solution I shown in Section 2.1.1, a problem of a conducting solid with two interior temperature sensors located at points $x = \chi_L$ (left hand sensor) and $x = \chi_M$ (right hand sensor) as shown in figure 2.1. The solid has two dimensionless specified surfaces at $x = 0$ and $x = \chi_N = 1$. These two sensors are movable between $x = 0$ and $x = \chi_N = 1$ (the left hand boundary and the right hand boundary of the computational domain respectively).

The IHCP considered in this chapter is shown in figure 2.1. It is assumed that

the temperature data at the two interior sensor locations $x = \chi_L$ and $x = \chi_M$ are taken from equation (2.5). The inverse problem is to find the unknown time histories of the temperatures and heat fluxes at the left hand boundary of the solid $x = 0$ and at the right hand boundary of the computational domain $x = \chi_N = 1$. The numerical reconstruction results at $x = 0$ and $x = \chi_N = 1$ are then compared with those of the exact solution, equation (2.5), to obtain the error percentages at $x = 0$ and $x = \chi_N = 1$ caused by the change of the sensor locations.

4.3 Numerical Experiments

A fully implicit finite difference scheme of equations (2.12)-(2.20) will be used in numerical simulation to indicate that the error of the reconstruction temperature at the left and right hand boundaries, which can be simplified by the following relations:

- At the left hand boundary, $x = 0$,

$$\sigma_{LH}(\%) = \Lambda_{LH} \cdot \chi_L \cdot \chi_M \tag{4.1}$$

- At the right hand boundary of the computational domain, $x = 1$,

$$\sigma_{RH}(\%) = \Lambda_{RH} \cdot (1 - \chi_L) \cdot (1 - \chi_M) \tag{4.2}$$

where

$$0 < \chi_L < \chi_M < 1 \tag{4.3}$$

The coefficients Λ_{LH} and Λ_{RH} can be determined by using one numerical simulation of a pair of specified sensor locations at $x = \chi_L^*$ and $x = \chi_M^*$ to obtain σ_{LH}^* and σ_{RH}^*. Due to the ill-posed condition of the inverse problem, the distance between the two sensor locations at $x = \chi_L^*$ and $x = \chi_M^*$ should be taken as far apart as possible (Hensel, 1991). In the present study, the distance between the two sensor locations should not be closer than 0.05 in dimensionless scale, *i.e.* $|\chi_L^* - \chi_M^*| \geq 0.05$.

The coefficients, Λ_{LH} and Λ_{RH}, can then be determined from equations (4.1)-(4.2) as follows:

$$\Lambda_{LH} = \frac{\sigma_{LH}^*}{\chi_L^* \cdot \chi_M^*} \tag{4.4}$$

$$\Lambda_{RH} = \frac{\sigma_{RH}^*}{(1 - \chi_L^*) \cdot (1 - \chi_M^*)} \tag{4.5}$$

To confirm the error relations presented in equations (4.1)-(4.2), the following four temperature functions for the boundary condition $f(t)$ appearing in equation (2.3) will be used.

- **Case 1**: A linear function ($a_1 > 0$)

$$f(t) = a_1 t \tag{4.6}$$

- **Case 2**: A quadratic function ($b_1 \geq 0, b_2 > 0$)

$$f(t) = b_1 t + b_2 t^2 \tag{4.7}$$

- **Case 3**: An exponential function ($c_1 > 0, c_2 > 0$)

$$f(t) = c_1 e^{c_2 t} \tag{4.8}$$

- **Case 4:** A periodic function ($d_1 > 0, d_2 > 0, \omega > 0$)

$$f(t) = d_1 + d_2 \sin(\omega \cdot t) \tag{4.9}$$

To determined the coefficients Λ_{LH} and Λ_{RH}, numerical values of a_1, b_1, b_2, c_1, c_2, d_1, d_2, and ω appearing in equations (4.6) to (4.9) must be fixed. With mesh size $\Delta x = 0.05$, $\Delta t = 0.05$, the selected parameter values of the functions and the calculated results of σ^*_{LH} , σ^*_{RH} , Λ_{LH}, Λ_{RH}, and two specified sensor locations are summarized as follows:

- **Case 1:** A linear function

$$\begin{array}{llllll} a_1 = 50 & ; & \chi^*_L = 0.35 & ; & \sigma^*_{LH} = 1.070 & ; \quad \Lambda_{LH} = 4.703 \\ & & \chi^*_M = 0.65 & & \sigma^*_{RH} = 1.218 & \quad \Lambda_{RH} = 5.354 \end{array}$$

The recovery errors at the left and right hand boundaries, from equations (4.1) and (4.2), are:

$$\sigma_{LH}(\%) = 4.703 \cdot \chi_L \cdot \chi_M \tag{4.10}$$

$$\sigma_{RH}(\%) = 5.354 \cdot (1 - \chi_L) \cdot (1 - \chi_M) \tag{4.11}$$

- **Case 2:** A quadratic function

$$\begin{array}{llllll} b_1 = 50 & ; & \chi^*_L = 0.35 & ; & \sigma^*_{LH} = 1.373 & ; \quad \Lambda_{LH} = 6.035 \\ b_2 = 2 & & \chi^*_M = 0.65 & & \sigma^*_{RH} = 1.563 & \quad \Lambda_{RH} = 6.870 \end{array}$$

The recovery errors at the left and right hand boundaries, from equations (4.1) and (4.2), are:

$$\sigma_{LH}(\%) = 6.035 \cdot \chi_L \cdot \chi_M \tag{4.12}$$

$$\sigma_{RH}(\%) = 6.870 \cdot (1 - \chi_L) \cdot (1 - \chi_M) \tag{4.13}$$

- **Case 3**: An exponential function

$c_1 = 50$; $\chi_L^* = 0.35$; $\sigma_{LH}^* = 2.649$; $\Lambda_{LH} = 11.644$
$c_2 = 2$ $\chi_M^* = 0.65$ $\sigma_{RH}^* = 3.015$ $\Lambda_{RH} = 13.252$

The recovery errors at the left and right hand side boundaries, from equations (4.1) and (4.2), are:

$$\sigma_{LH}(\%) = 11.644 \cdot \chi_L \cdot \chi_M \tag{4.14}$$

$$\sigma_{RH}(\%) = 13.252 \cdot (1 - \chi_L) \cdot (1 - \chi_M) \tag{4.15}$$

- **Case 4**: A periodic function

$d_1 = 150$; $\chi_L^* = 0.35$; $\sigma_{LH}^* = 2.868$; $\Lambda_{LH} = 12.606$
$d_2 = 40$ $\chi_M^* = 0.65$ $\sigma_{RH}^* = 3.264$ $\Lambda_{RH} = 14.347$
$\omega = 2.5$

The recovery errors at the left and right hand side boundaries, from equations (4.1) and (4.2), are:

$$\sigma_{LH}(\%) = 12.606 \cdot \chi_L \cdot \chi_M \tag{4.16}$$

$$\sigma_{RH}(\%) = 14.347 \cdot (1 - \chi_L) \cdot (1 - \chi_M) \tag{4.17}$$

Figures 4.1, 4.3, 4.5, and 4.7 show the errors in temperature recovery at the left hand boundary, $x = \chi_o = 0$, as a function of the right hand sensor location with the left hand sensor location as a parameter for cases 1 to 4, respectively. Similarly, Figures 4.2, 4.4, 4.6, and 4.8 show the errors in temperature recovery

at the right hand boundary, $x = \chi_N = 1$, as a function of the right hand sensor location with the left hand sensor location as a parameter for cases 1 to 4, respectively. The symbols and lines appearing in Figures 4.1 to 4.8 are the values calculated by the inverse solver presented in section 3, and by simplified relations, equations (4.10) to (4.17), respectively. The differences between the results obtained from the simplified relations, equations (4.10) to (4.17), and the results calculated by the inversion solver are very small, within a relative error of 0.5%.

4.4 Summary

From numerical calculations the following conclusions can be drawn:

1. The errors of the reconstruction temperature at the left and right hand boundaries, caused by the variation of the two sensors located in $0 < \chi_L < \chi_M < 1$ of a one-dimensional IHCP, can be approximately determined by the simple relations, (4.1) and (4.2), respectively.

2. Equations (4.1) and (4.2) are confirmed by the selected four temperature functions, equations (4.6) to (4.9). The characteristics of the errors of the reconstruction temperatures are summarized by the numerical simulation as follows:

   - Case 1, the linear function, equation (4.6):

     Equations (4.10) and (4.11) are available for any positive value of a_1.

- Cases 2 and 3, the quadratic and exponential functions, equations (4.7) and (4.8), respectively:

  For cases 2 and 3, the larger the temperature slope, $\frac{df(t)}{dt}$, at $x = 0$, the larger are the errors of the reconstruction temperatures at the both side boundaries.

- Case 4, the periodic function, equation (4.9):

  For a given value of ω in the range of $0 < \omega < 5$ in equation (4.9), the larger is the ratio of $\frac{d_2}{d_1}$, the larger are the errors of the reconstruction temperatures at the both side boundaries.

3. The numerical simulation results show that the effect of time on the temperature recovery error is negligibly small.

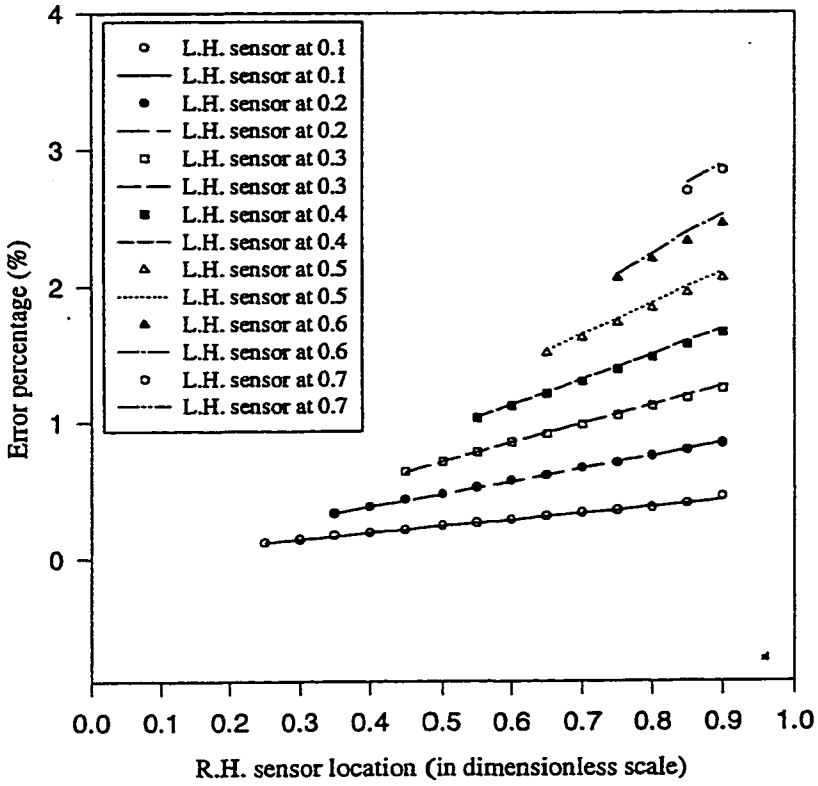

Figure 4.1: Temperature recovery error at the L.H. boundary as a function of the R.H. sensor location for case 1 with the L.H. sensor location as parameter.

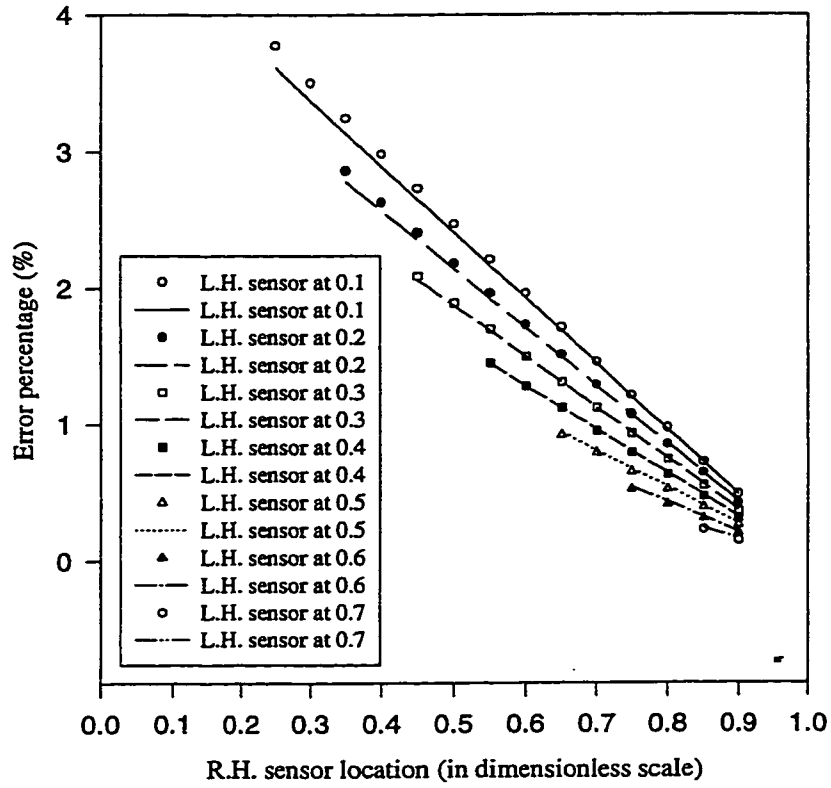

Figure 4.2: Temperature recovery error at the R.H. boundary as a function of the R.H. sensor location for case 1 with the L.H. sensor location as parameter.

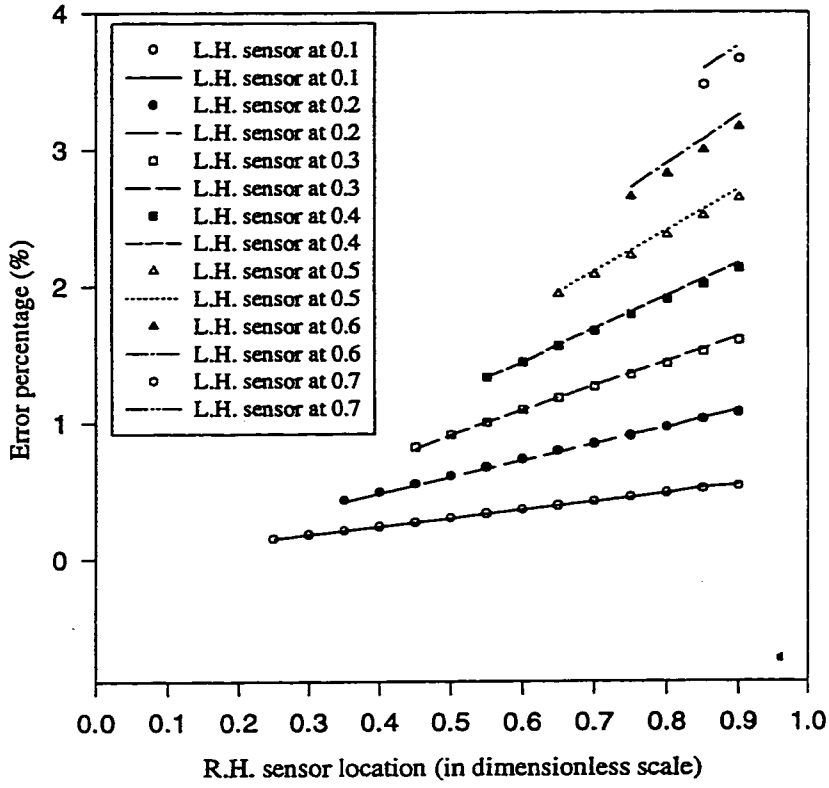

Figure 4.3: Temperature recovery error at the L.H. boundary as a function of the R.H. sensor location for case 2 with the L.H. sensor location as parameter.

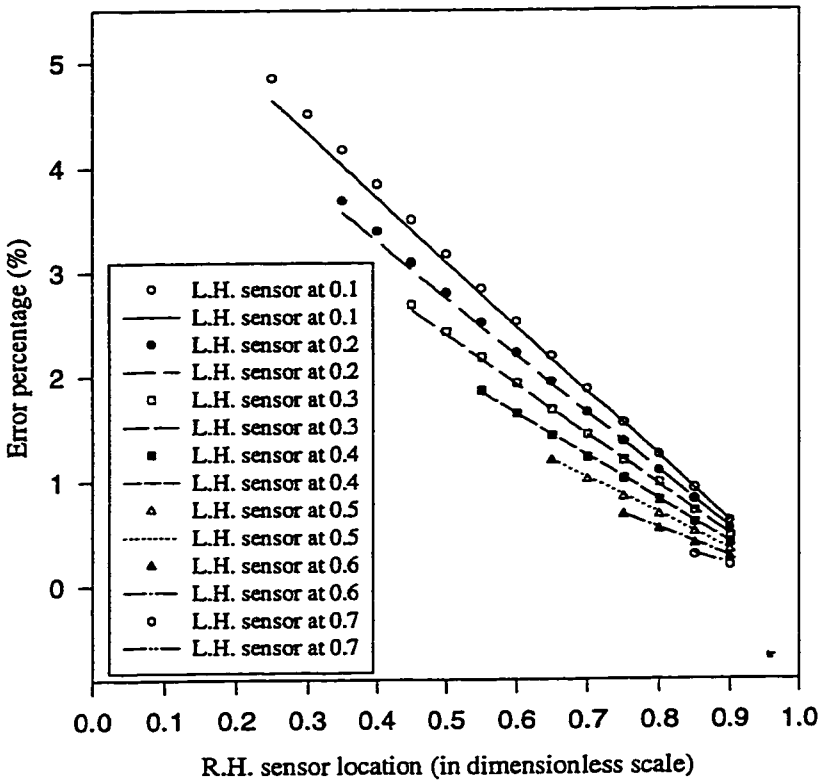

Figure 4.4: Temperature recovery error at the R.H. boundary as a function of the R.H. sensor location for case 2 with the L.H. sensor location as parameter.

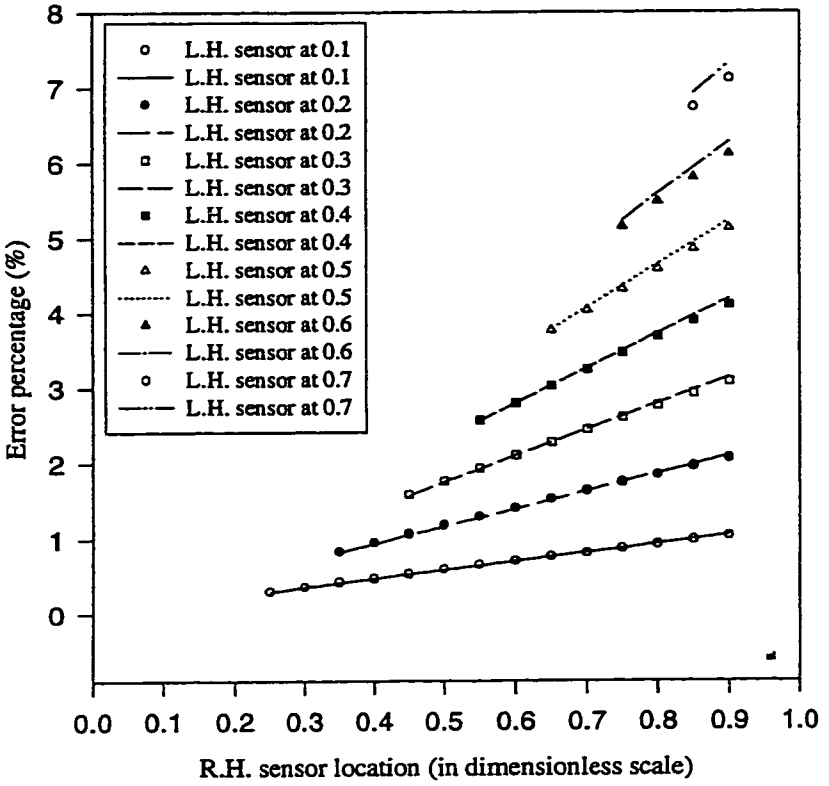

Figure 4.5: Temperature recovery error at the L.H. boundary as a function of the R.H. sensor location for case 3 with the L.H. sensor location as parameter.

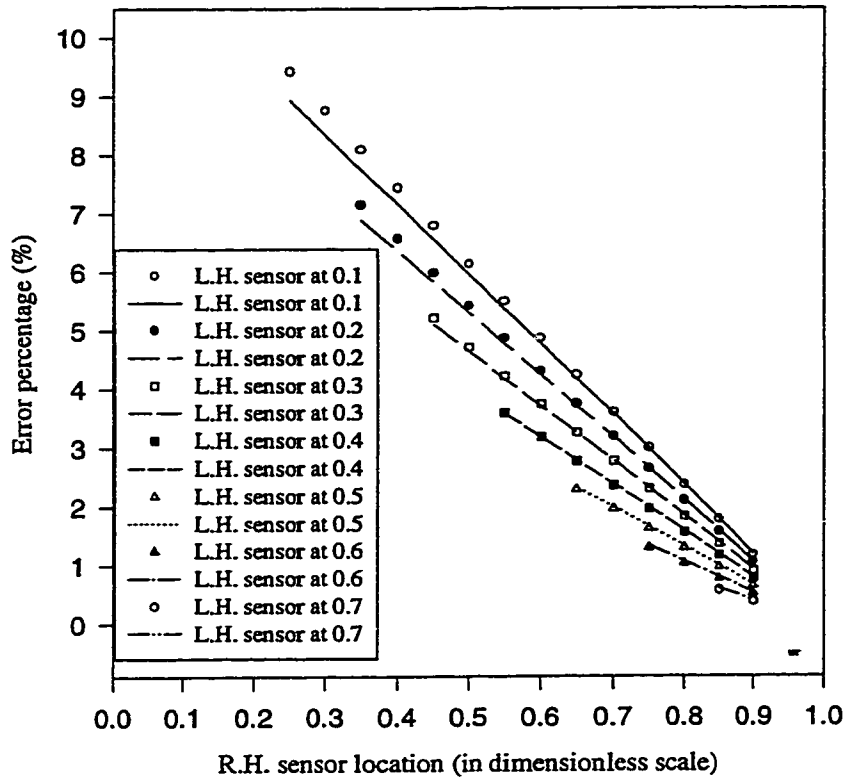

Figure 4.6: Temperature recovery error at the R.H. boundary as a function of the R.H. sensor location for case 3 with the L.H. sensor location as parameter.

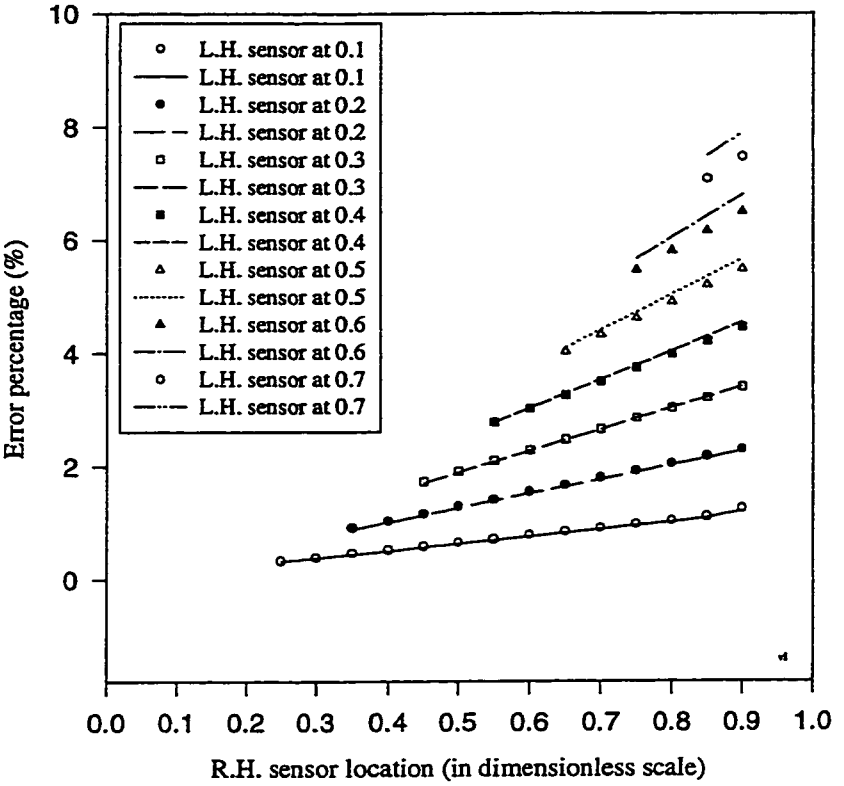

Figure 4.7: Temperature recovery error at the L.H. boundary as a function of the R.H. sensor location for case 4 with the L.H. sensor location as parameter.

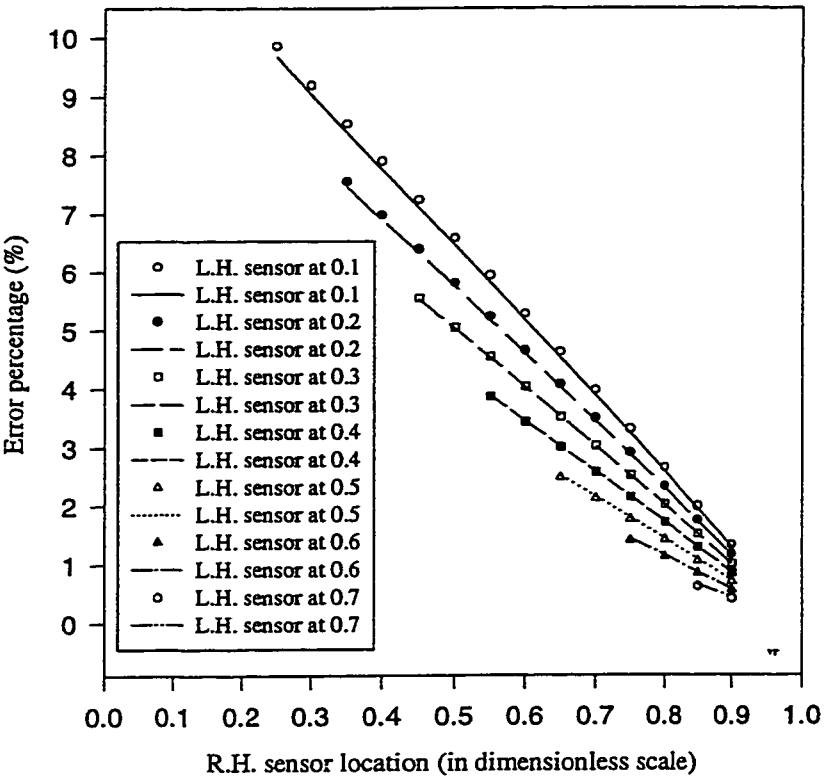

Figure 4.8: Temperature recovery error at the R.H. boundary as a function of the R.H. sensor location for case 4 with the L.H. sensor location as parameter.

Chapter 5

Experimental Work

In parallel to the foregoing inversion solver to recover surface temperatures and heat fluxes, the inversion model has also been studied experimentally. The experimental work is presented in this chapter.

5.1 Experimental Objectives

Experiments will validate the theory and numerical solver which has been developed for the space boundary IHCP in the foregoing chapter. For this purpose, a one-dimensional heat conduction experiment with thermocouple monitoring the temperature profile is designed in order to compare with the numerical recovery results. Through the temperatures from the interior measurement sensors, we recover the boundary temperatures and heat fluxes, and compare with the experimental results at the both side boundaries. The objectives of the present experiments are

as follows:

1. to reconstruct the boundary conditions by inversion solver;
2. to compare the error of the recovery results with experimental data; and
3. to establish an application of a boundary inverse heat conduction problem, and to determine the adaptivity and flexibility of the present inversion solver.

5.2 Experimental Setup

Figure 5.1 shows the experimental apparatus (Lin and Chen, 1996, 1997) which simulates the temperature profile of a furnace wall made of two bricks connected longitudinally. This apparatus can be separated into three major parts: metal box, radiation heater and data acquisition system. The metal box, mounted on an aluminum cross-beam base, can contain two bricks. An insulation material is used around the outside of the two bricks to form a one-dimensional heat flux process.

The two bricks in the metal box are heated by a radiation heater (figure 5.2) located on the left hand side of the test apparatus in figure 5.1. This radiation heater can heat up to $700°C$. The temperature of the brick located close to the heater (*i.e.* left hand side of the test apparatus in figure 5.1) is higher than that of the other brick (*i.e.* right hand side of the test apparatus). Ten copper-constantan thermocouples (figures 5.3 and 5.4) monitor the temperature profile along the test bricks in the metal box. The temperature at the heating surface of the test brick

is controlled by a temperature controller which can provide a desired temperature. Each temperature signal obtained from these ten thermocouples is recorded by the data acquisition system (figures 5.5, 5.6).

5.3 Tasks of the Experiment

The experiments are designed to compare accuracy of the recovery results and the temperature drop between two contacting bricks with the boundary inversion solver developed in section 2.2. The experimental tasks are defined as follows:

- Task 1: Single brick experiment, to test the accuracy of the recovery results by the inversion solver at the boundary.
- Task 2: Two bricks experiment, to reconstruct the temperature drop between two roughness interface surfaces.

The experimental conditions are shown in Table 5.1, where test runs **1**, **3**, and **4** are for Task 1, and test runs **2** and **5** are for Task 2.

Run	Test bricks	Effective region	Surface temperature	Heating time
1	one	4.76 cm → 27.7 cm	23 °C → 250 °C	149 mins
2	two	4.76 cm → 73.2 cm	23 °C → 317 °C	346 mins
3	one	4.76 cm → 27.7 cm	350 °C → 400 °C	72 mins
4	one	4.76 cm → 27.7 cm	350 °C → 410 °C	140 mins
5	two	4.76 cm → 73.2 cm	28 °C → 350 °C	170 mins

Table 5.1: Summary of experimental conditions

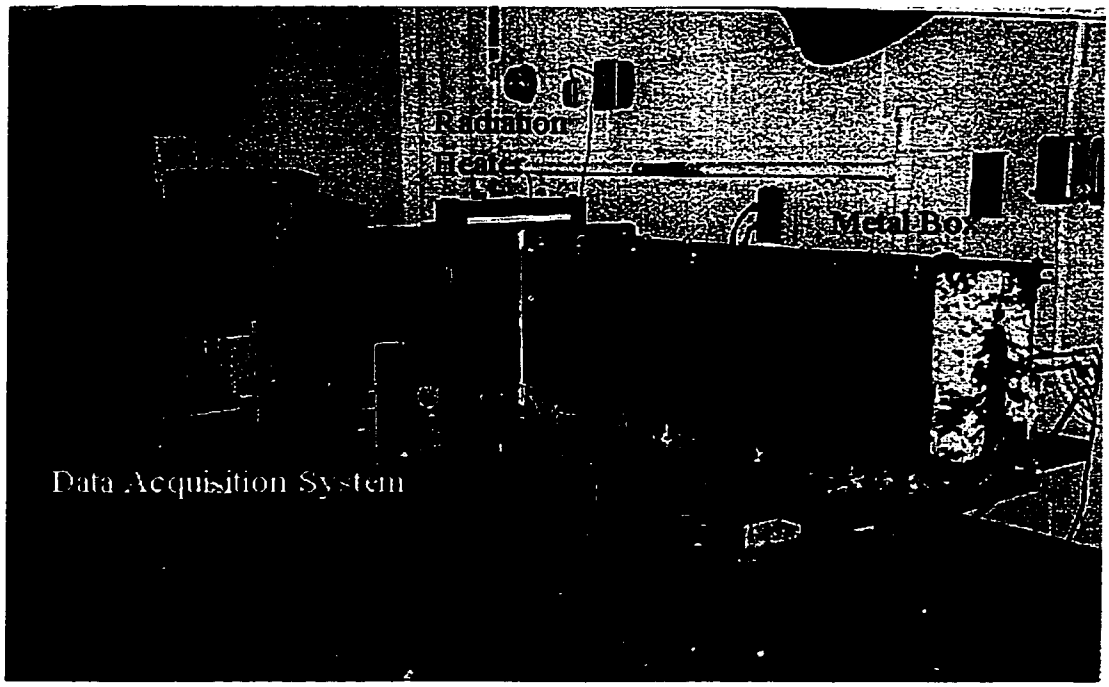

Figure 5.1: Experimental setup

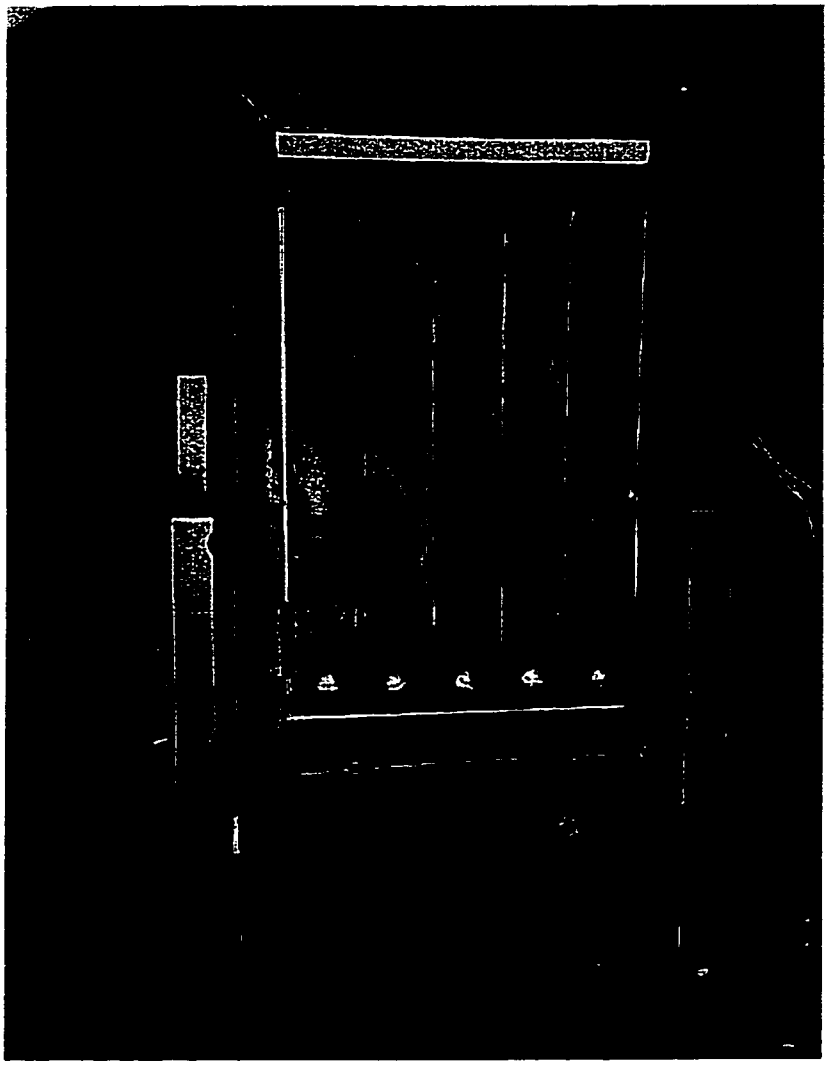

Figure 5.2: Radiation heater

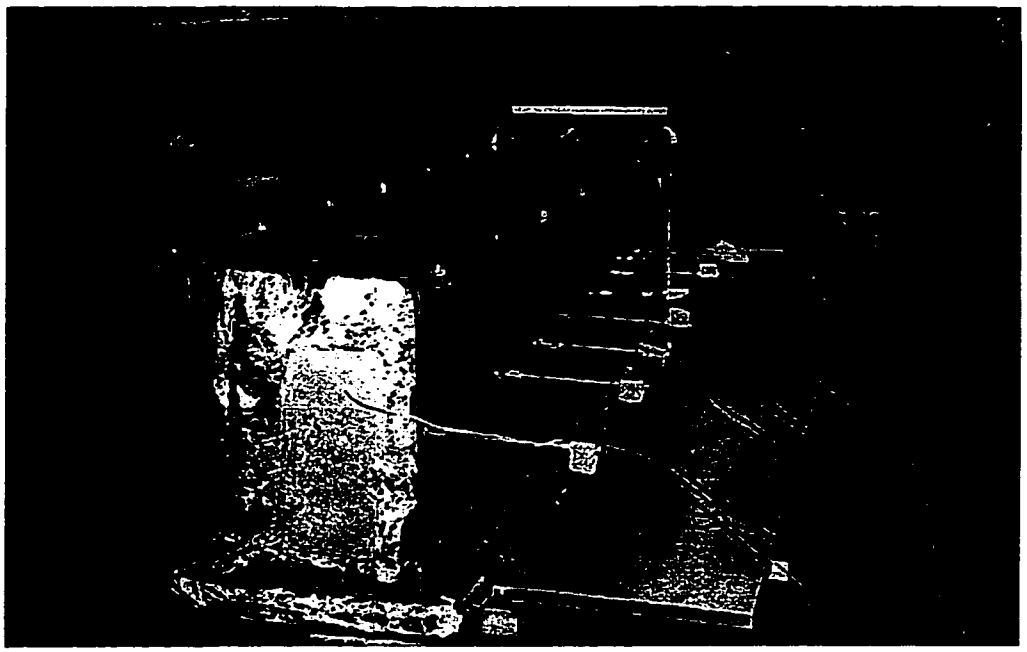

Figure 5.3: Ten copper constantan thermocouples

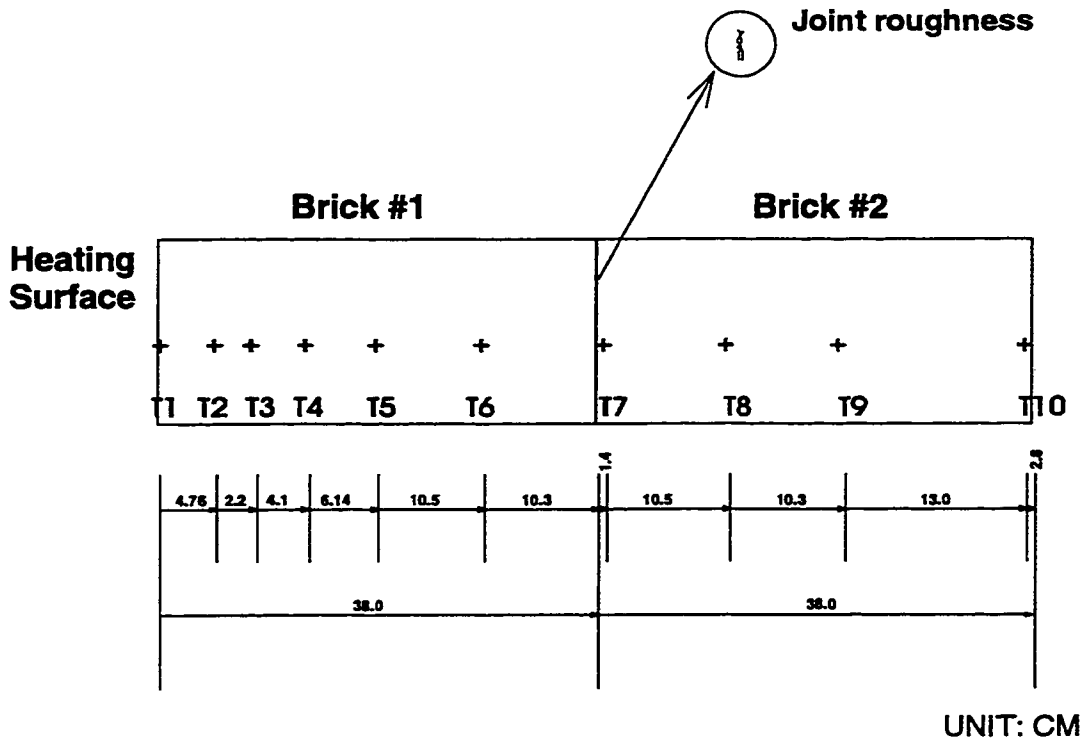

Figure 5.4: Thermocouple setup

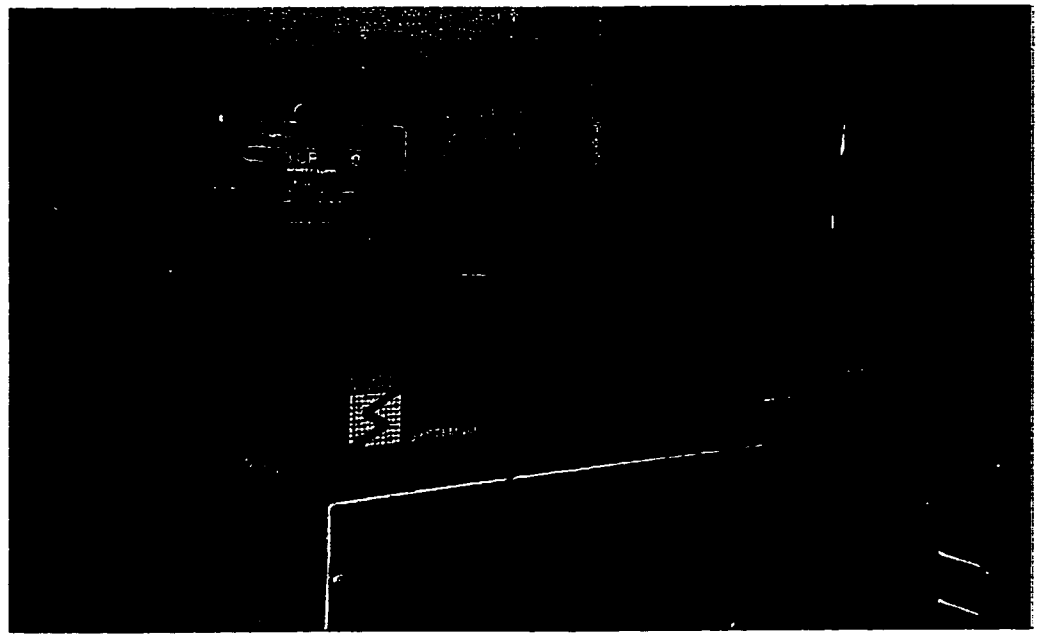

Figure 5.5: Data acquisition system

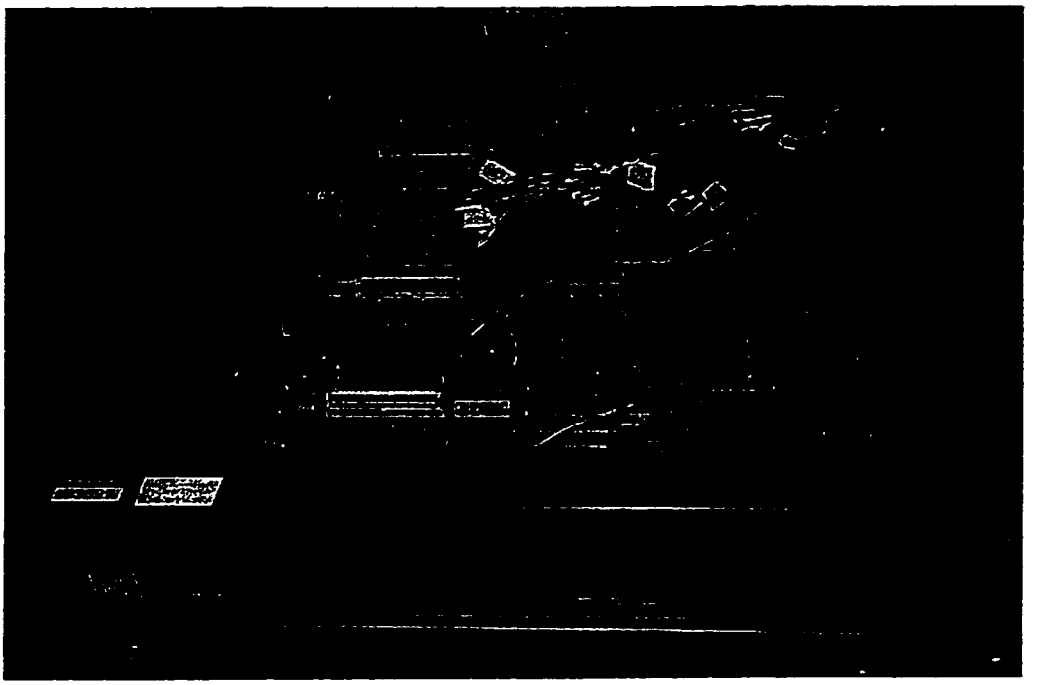

Figure 5.6: Breakdown of the data acquisition system

Chapter 6

Recovery Results of Experiments

In this chapter, boundary reconstruction temperatures will be validated with experimental data. First, we compare the reconstruction surface temperature through the inversion solver (Chen *et al.*, 1996) described in Section 2.2 with the recorded temperature data of the one brick experiment. Second, the temperatures of the two contiguous boundary surfaces of two contact bricks are recovered by the inversion procedures, and the temperature drop due to the thermal contact resistance between the two bricks can be obtained through the recovery results of the two contiguous surfaces. Errors of the reconstruction temperatures of each sensor location will be demonstrated in the following sections.

6.1 One-brick Boundary Recovery Temperature

The experimental thermocouple setup is shown in figure 5.4. Here we present a real space IHCP by using the inversion solver described in Section 2.2 to reconstruct the boundary temperatures. For the one-brick case (*i.e.* inside brick #1 region), we choose the computation domain shown in figure 6.1. Use T3 and T5 temperature measurement data to recover left hand and right hand boundary temperatures (*i.e.* T2 and T6 respectively). Because we have temperature measurements at positions T2 and T6, we can compare the recovery boundary temperatures with the experimental results to obtain the temperature recovery errors.

For the numerical calculation, the following data will be chosen:

1. Dimensions of the brick: $38cm \times 7.6cm \times 15.1cm$
2. Computational domain starts from thermocouple T2 position (left boundary) to T6 position (right boundary). Total computational domain is $22.94cm$ (*i.e.* $4.76cm$ to $27.70cm$ from heating surface).
3. $\Delta x = 1.147cm$
4. $\Delta t = 0.1sec$
5. Specific heat of the experiment brick, $c_p \cong 0.88kJ/kg \cdot^\circ C$
6. Brick density $\rho \cong 2867kg/m^3$

7. Thermal conductivity of the brick is shown in figure 6.2.

8. Experimental test condition is taken as the test run **1** indicated in Table 5.1 which is selected for numerical reconstruction.

9. Initial temperature for starting the inverse process is interpolated from the thermocouples' output in the experiment at the test time $t = 64.32\,\text{min}$ by the cubic spline method and is shown in figure 6.3.

Use the thermal conductivity of the brick as a temperature function to recover the temperature results. Figure 6.4 describes the recovered temperature results at the right and left hand boundaries in comparison with the experimental data, and the recovery errors are shown in figure 6.5. The recovery temperature in the computational domain is shown in figure 6.6 at $t = 400sec.$ From these figures, it is shown that the results of the reconstruction temperatures are very close to the experimental data. The relative errors between them are within 2.0%.

6.2 Recovery Temperature Drop Due to Thermal Resistance

6.2.1 Background

Since there is no actual perfectly smooth surface, the interface between two solid surfaces should consist of a resistance to heat flow and a temperature drop (ΔT)

when two surfaces fit tightly together. This kind of interface resistance between two surfaces is called contact resistance. The determination of contact resistance is interesting because many industrial thermal systems or furnace insulations have components like bolted and riveted joints, connectors, hinges, brick connection, *etc.* The field of thermal contact resistance has been widely investigated by numerous researchers, for examples, Clausing and Chao (1965), Forslund and Oliveira (1975), Thomas (1975), Yovanovich *et al.* (1976), Özişik (1977), Wang (1981), Mikic (1982), Shai and Santa (1982), and Kreith and Bohn (1986) *etc.* For solving the thermal resistance problem, various models have been utilized by researchers for theoretical and experimental prediction of the temperature difference between two contacting surfaces. Most of these results are based on the steady state heat flow condition.

In this section, we use a space boundary inversion scheme (Chen *et al.,* 1996) to predict the two interface temperatures. The transient non-stationary temperature drop (ΔT) between the two surfaces can be determined.

6.2.2 Numerical Recovery Results

The experimental thermocouple setup is shown in figure 5.4. Here we present an inversion scheme (Chen *et al.,* 1996) to reconstruct the temperatures at the both sides of the contiguous surfaces between two bricks. For the region of bricks #1 and #2, we choose the computation domain as shown in figure 6.7. Using the thermocouples T5 and T6 inside brick #1, and T8, T9 inside brick #2, we recover

the interface surface temperatures on brick #1's right hand side and brick #2's left hand side. The interface temperature drop (ΔT) can then be obtained.

For the numerical calculation, the following data are chosen:

1. Dimensions of two bricks: $76cm \times 7.6cm \times 15.1cm$
2. There are two inversion computational domains as follows,
   - For brick #1, start from thermocouple T2 position to the end of the right hand side of the brick. Total computational domain is 33.24 cm (*i.e.* 4.76 cm to 38.00 cm from the heating surface).
   - For brick #2, start from the left hand side of brick #2 to the position 33.24 cm from the beginning of brick #2. Total computational domain is 33.24 cm (*i.e.* 38 cm to 71.24 cm from the heating surface).
3. $\Delta x = 1.662$ cm
4. $\Delta t = 0.1$ sec
5. Specific heat of the bricks, $c_p \cong 0.88kJ/kg \cdot^\circ C$
6. Brick density $\rho \cong 2867kg/m^3$
7. Thermal conductivity of the brick is shown in figure 6.2.
8. Experimental test condition is taken as the test run **2** indicated in Table 5.1, which is selected for numerical reconstruction.

9. Initial temperatures of the two bricks for starting the inverse process are interpolated from the thermocouples' output in the experiment at the test time $t = 121.84\,\text{min}$ by the cubic spline method.

The calculation procedures for the temperature drop recovering simulation are as follows,

1. Reconstruct the left and right boundary temperatures in brick #1 through T5, T6 temperature measurements.
2. Reconstruct the left and right boundary temperatures in brick #2 through T8, T9 temperature measurements.
3. The temperature difference between the right boundary temperature in brick #1 and the left boundary temperature in brick #2 is the temperature drop (ΔT) between the two contact bricks due to thermal resistance.

Figure 6.8 shows the temperature recovery results of bricks #1 and #2 in comparison with the experimental data at $t = 400sec$. Figure 6.9 shows the errors of the recovery temperatures in comparison with the experimental data obtained by the thermocouples T2, T3, T4 and T7 respectively. Figure 6.10 shows the time variation of the recovering temperature drop (ΔT) between the two contact bricks. At the time $t = 400sec$, the recovering temperature drop (ΔT) is about $10°C$ as shown also in figure 6.8.

6.3 Summary

The inversion solver developed can reconstruct well the unknown boundary temperatures of the experimental heating single brick. This inversion solver can also predict the thermal contact resistance between the two contact bricks.

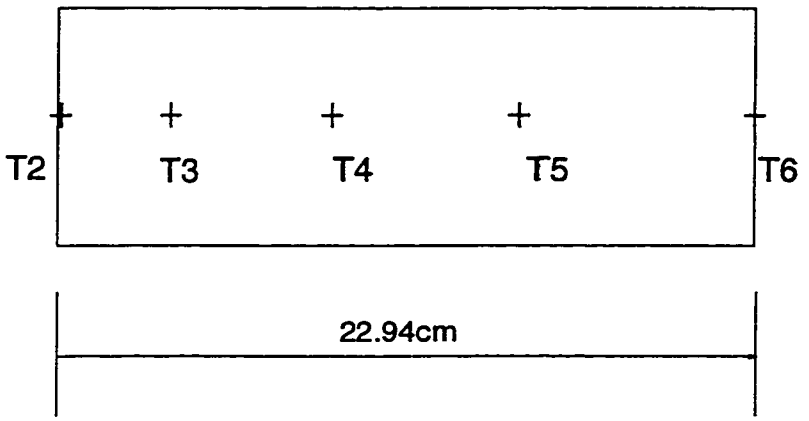

Inverse model:
- Two interior measurement temperatures (T3, T5)
- Recover unknown boundaries at positions T2 and T6, then compare the recovered boundary temperatures with the experimental monitoring results at positions T2 and T6

Mesh size:
- $\Delta x = 1.147$ cm
- $\Delta t = 0.1$ sec

Figure 6.1: Computational domain for the single-brick experiment

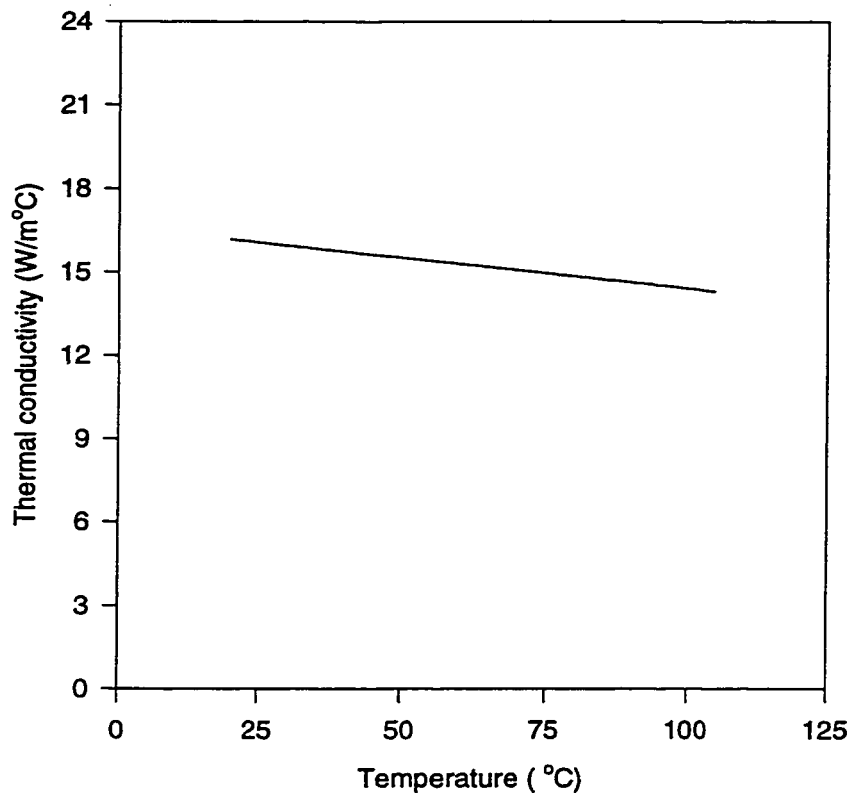

Figure 6.2: Thermal conductivity of the brick (manufacturer's data)

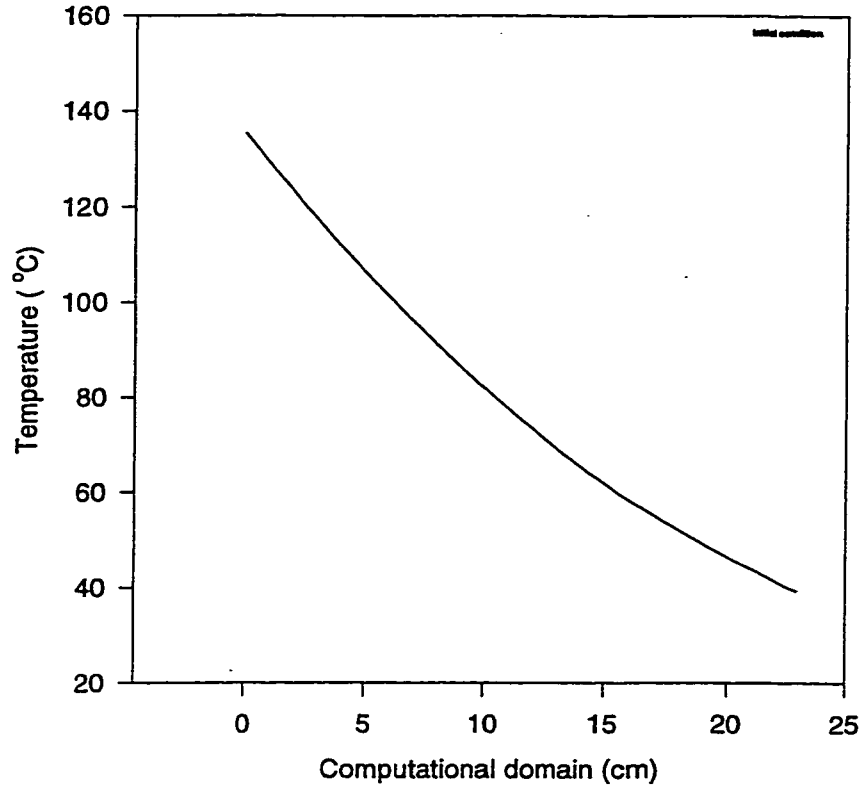

Figure 6.3: Initial condition for numerical simulation

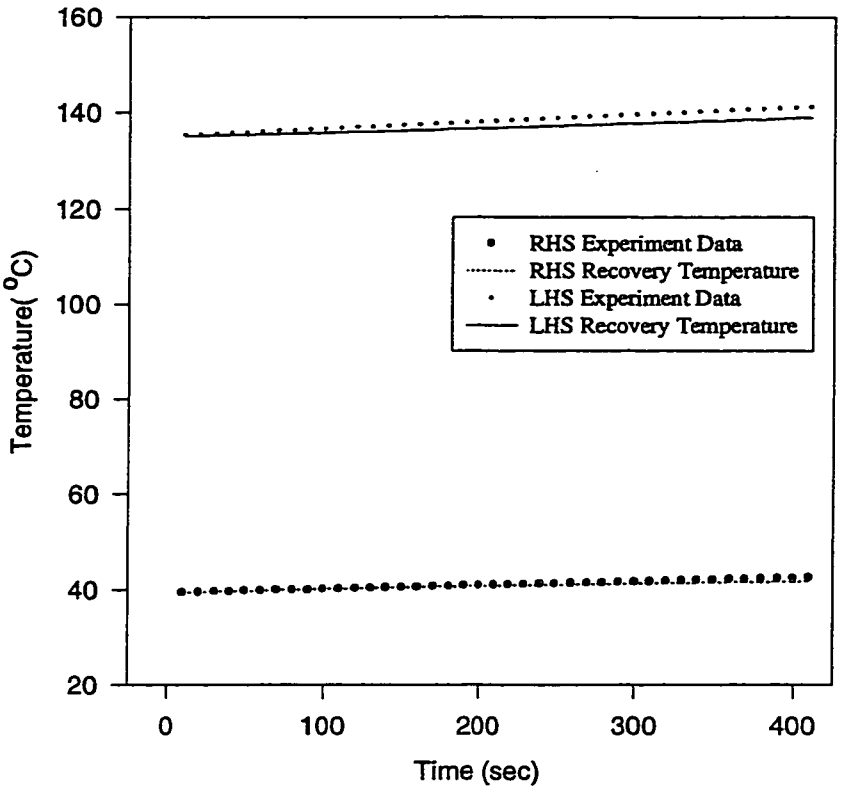

Figure 6.4: RHS and LHS boundary temperature recovery results in comparison with experimental data

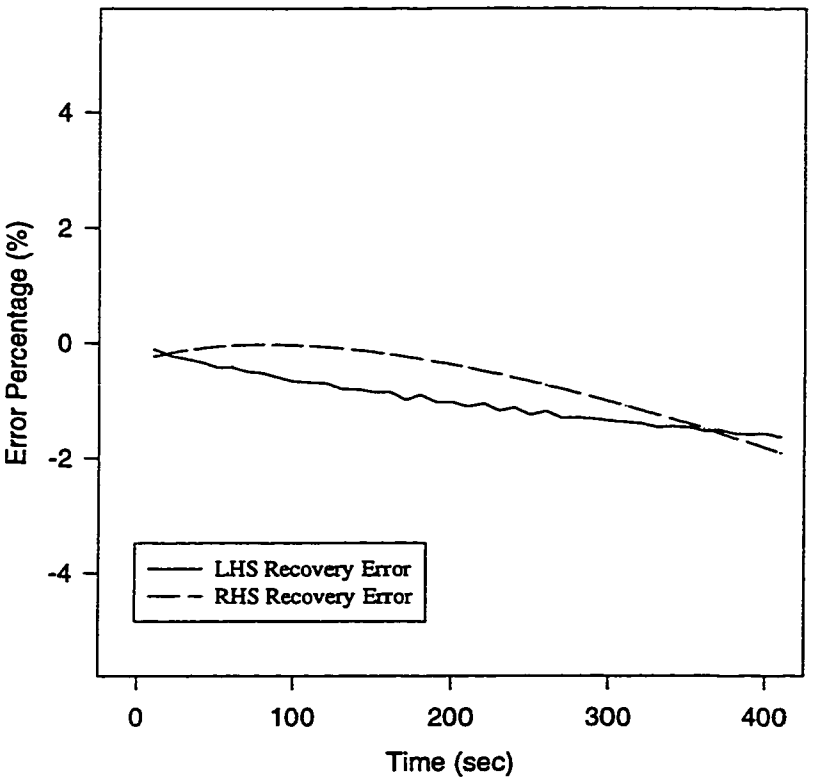

Figure 6.5: Relative errors of the RHS and LHS boundary recovery temperatures

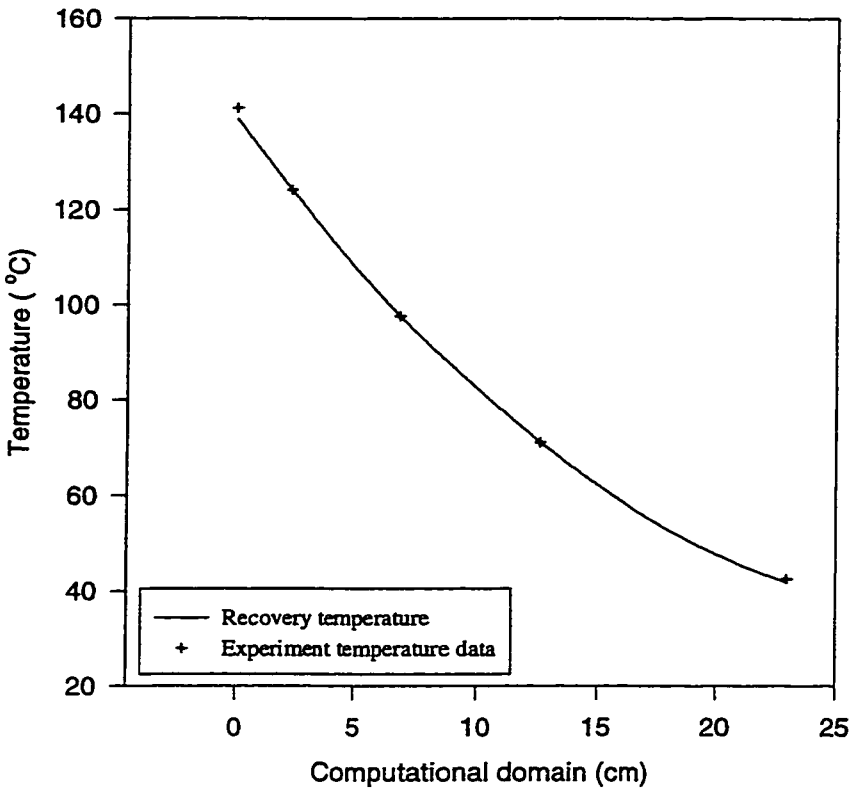

Figure 6.6: Recovery temperature and experiment data of the test domain at $t = 400sec$

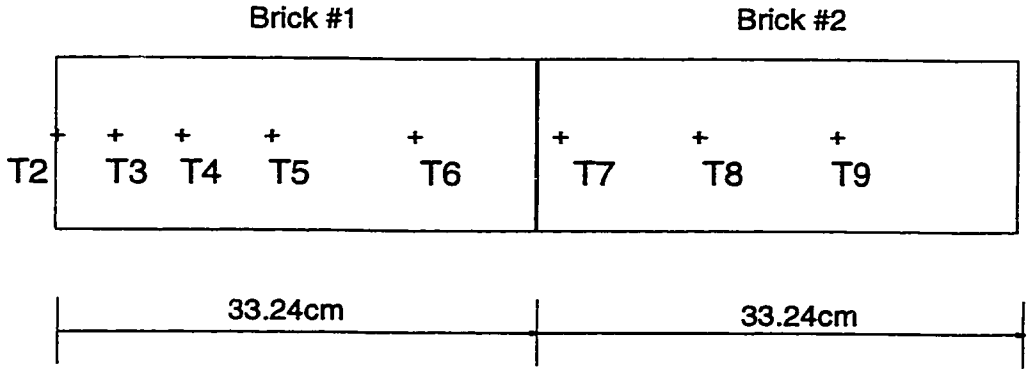

Inverse model:
- Two interior measurement temperatures (T5, T6) in Brick #1 and (T8, T9) in Brick #2, respectively
- Recover two unknown boundary temperatures in Bricks #1 and #2, respectively
- Obtain temperature drop (ΔT) from Brick #1 RHS and Brick #2 LHS boundary temperatures

Mesh size:
- $\Delta x = 1.662$ cm
- $\Delta t = 0.1$ sec

Figure 6.7: Computational domain for the two-brick experiment

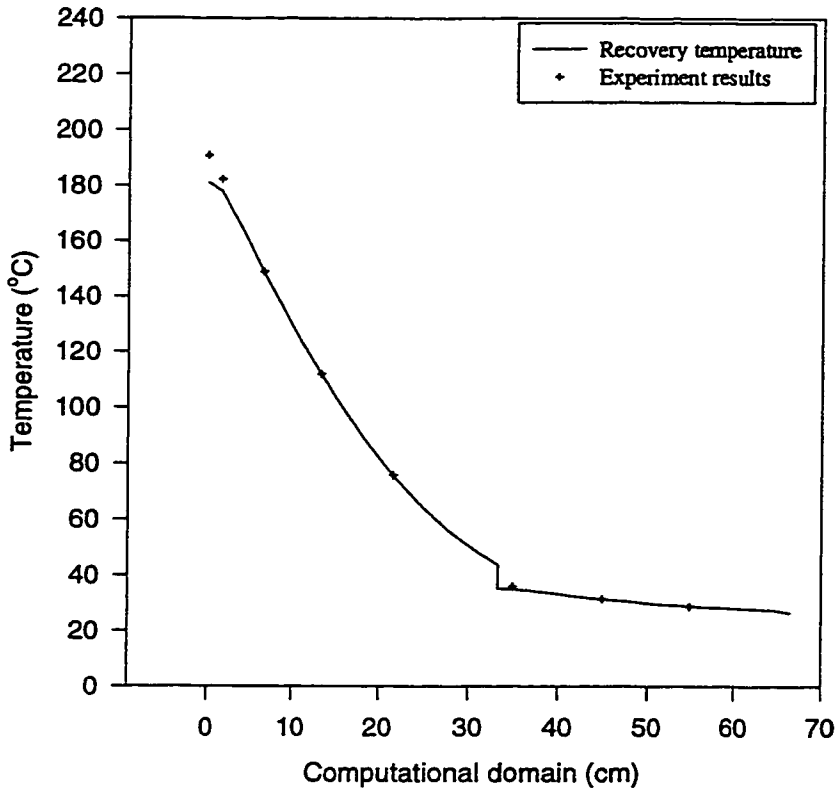

Figure 6.8: Recovery temperatures in comparison with experiment data of test domain bricks #1 and #2 at $t = 400sec$

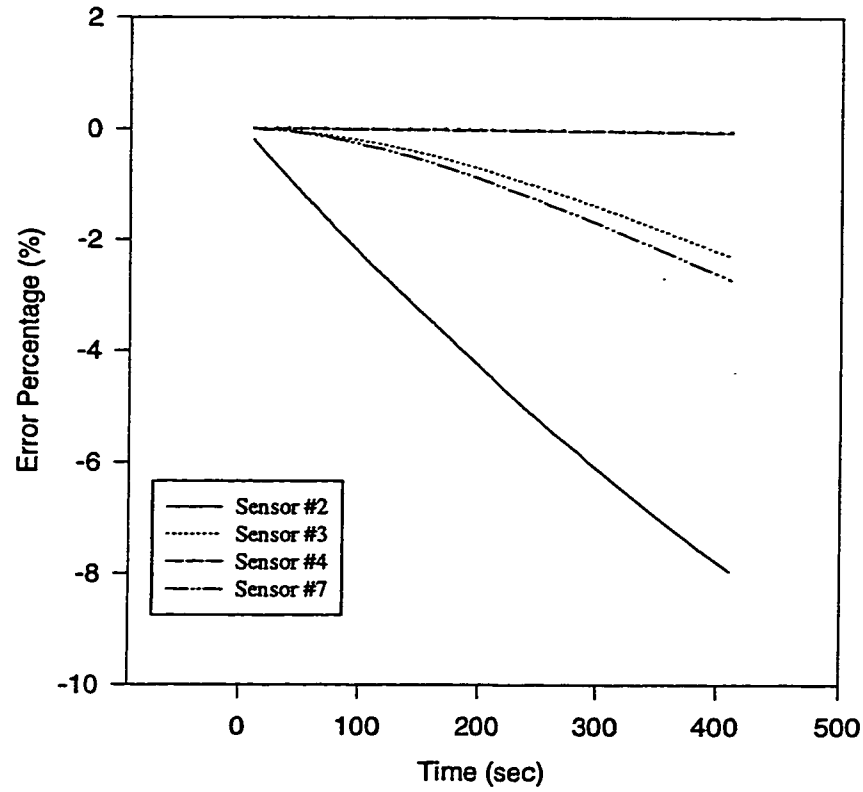

Figure 6.9: Recovery temperature errors at different measurement points

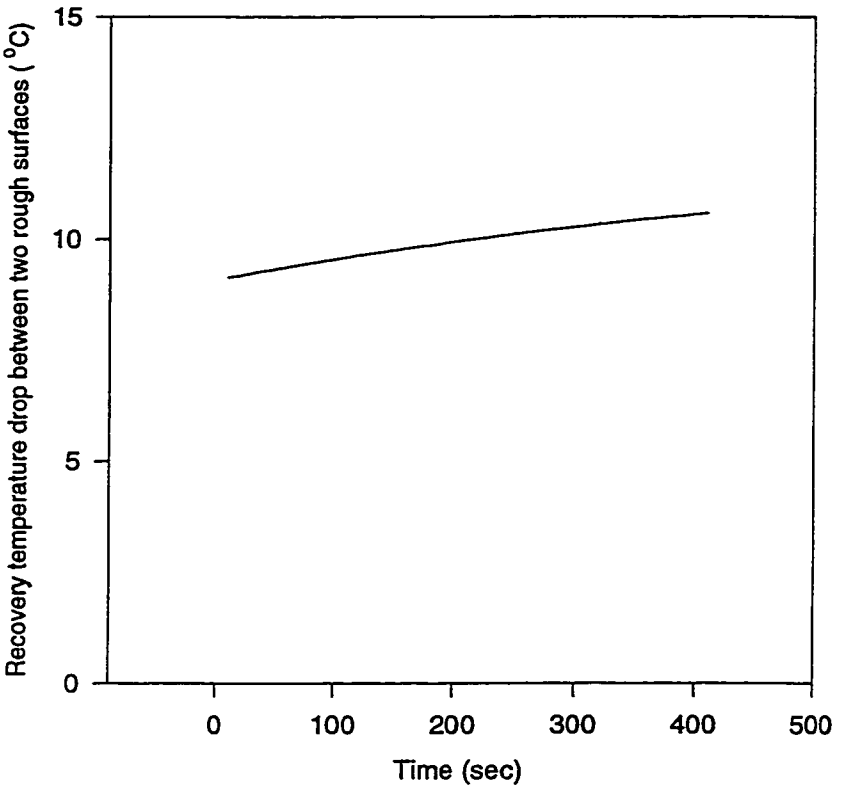

Figure 6.10: Transient recovery temperature drop between two rough surfaces

Chapter 7

A Flux Limiter Finite Difference Scheme in Solving a One-Dimensional Inverse Stefan Problem

7.1 Introduction

This chapter presents an enthalpy formulation of a finite difference scheme for solving an inverse Stefan problem in one space variable. When measurements cannot access the inside of the intended test domain, experimental information may be taken only from one side of the surface. The current inversion procedure considers one side surface boundary conditions (*i.e.* both the surface temperature and the heat flux at one side of the boundary) to recover the unknown interior temperature history and the melting front position. A semi-explicit time marching finite

difference scheme with a heat flux limiter (Chen *et al.*, 1997b) is used to handle the recovered temperature oscillation caused by the ill-posedness of the inverse problem, and to accelerate the rate of convergence. Numerical solution with and without the heat flux limiter are presented in comparison with an exact solution.

7.2 Mathematical Model of a Stefan Problem

Mathematical models of melting problems can be classified into two categories: the two-region approach and the single-region approach. In the two-region approach, the energy equation is separated for the solid and liquid phases. Each phase has its own governing equations, with the continuity of temperature and moving boundary conditions at the solid-liquid interface. In the single-region approach, the energy equation is modified and applied to both the solid and liquid regions. In this chapter an enthalpy method is used, neglecting the surface kinetics, the crystallization process at the interface, and the change in density across the moving phase front. The one-dimensional Stefan problem of melting a pure substance is defined as follows (Crank, 1984):

In the liquid region:

$$\rho_l(T)c_l(T)\frac{\partial T_l}{\partial t} = \frac{\partial}{\partial x}\left(k_l(T)\frac{\partial T_l}{\partial x}\right), t > 0, 0 < x < x_{melt}(t) \qquad (7.1)$$

In the solid region:

$$\rho_s(T)c_s(T)\frac{\partial T_s}{\partial t} = \frac{\partial}{\partial x}\left(k_s(T)\frac{\partial T_s}{\partial x}\right), t > 0, x_{melt}(t) < x < d \tag{7.2}$$

At the melting interface:

$$T_l(x_{melt}(t), t) = T_s(x_{melt}(t), t) = T_{melt} \tag{7.3}$$

With the Stefan condition (moving boundary condition):

$$k_s(T)\frac{\partial T_s}{\partial x} - k_l(T)\frac{\partial T_l}{\partial x} = \rho(T)L\frac{dx_{melt}(t)}{dt}, t > 0, x = x_{melt}(t) \tag{7.4}$$

Let $H(T)$ denote an enthalpy function with temperature variation; the enthalpy function (Crank, 1984) can be written as

$$H(T) = \int_{T_o}^{T} \rho(\Gamma)\left(c(\Gamma) + L\delta(\Gamma - T_{melt})\right) d\Gamma \tag{7.5}$$

where $T_o < T$.

The "weak" enthalpy formulation (Date, 1991) can be defined as follows:

$$\frac{\partial H}{\partial t} = \frac{\partial}{\partial x}\left(k(T)\frac{\partial T}{\partial x}\right) \tag{7.6}$$

or

$$\frac{\partial H}{\partial T}\frac{\partial T}{\partial t} = \frac{\partial}{\partial x}\left(k(T)\frac{\partial T}{\partial x}\right) \tag{7.7}$$

Equation (7.6) or (7.7) automatically satisfies equations (7.1) to (7.4).

From equation (7.5), an apparent heat capacity is defined as follows:

$$C^A(T) = \frac{\partial H(T)}{\partial T} = \rho(T)\left(c(T) + L\delta(T - T_{melt})\right) \tag{7.8}$$

Substituting equation (7.8) into equation (7.7) gives

$$C^A(T)\frac{\partial T}{\partial t} = \frac{\partial}{\partial x}\left(k(T)\frac{\partial T}{\partial x}\right) \tag{7.9}$$

7.3 One-dimensional Inverse Stefan Problem

The inverse Stefan problem considered in this chapter is shown in Figure 7.1. It is assumed that the material properties, the initial temperature, the melting temperature, the measured surface temperature and the heat flux at position $x = 0$ are known. The inverse problem is to find the time history of the temperature distributions in the solid and liquid regions, and the location of the melting front.

In order to introduce a heat flux term into equation (7.9), denote heat flux q as follows:

$$q = k(T)\frac{\partial T}{\partial x} \tag{7.10}$$

Equation (7.9) becomes

$$C^A(T)\frac{\partial T}{\partial t} = \frac{\partial q}{\partial x} \tag{7.11}$$

The initial and boundary conditions at the left-hand side ($x = 0$) are as follows:

$$T(x, 0) = T_i \tag{7.12}$$

$$T(0, t) = T_0(t) \tag{7.13}$$

$$q(0, t) = q_0(t) \tag{7.14}$$

The boundary condition at the right-hand side, $x = d$, is unknown. Due to this unknown boundary condition, the problem mentioned above, equations (7.11) to (7.14), cannot be solved directly. It is an inverse problem.

7.4 Numerical Scheme

For numerical calculation, equations (7.10) and (7.11) can be written in the following discrete form:

$$q_i^{n+1} = k(T)\frac{T_i^{n+1} - T_{i-1}^{n+1}}{\Delta x} \tag{7.15}$$

$$T_i^{n+1} = T_i^n + \frac{1}{C^A(T_i^n)}\frac{\Delta t}{\Delta x}\left(q_{i+\frac{1}{2}}^{n+1} - q_{i-\frac{1}{2}}^{n+1}\right) \tag{7.16}$$

Define

$$\lambda = \frac{1}{C^A(T_i^n)}\frac{\Delta t}{\Delta x} \tag{7.17}$$

where apparent heat capacity in equation (7.17), $C^A(T_i^n)$, can be approximated by the following function (Bonacina, 1973),

$$C^A(T) \doteq \begin{cases} \rho_s c_s, & T < T_{melt} - \epsilon \\ \left(\frac{\rho_s+\rho_l}{2}\right)\left(\frac{c_s+c_l}{2}\right) + \frac{\rho_s L}{2\epsilon}, & T_{melt} - \epsilon \le T < T_{melt} + \epsilon \\ \rho_l c_l, & T \ge T_{melt} + \epsilon \end{cases} \tag{7.18}$$

ϵ in equation (7.18) is a very small number. In this chapter, we choose $\epsilon = 0.1°C$.

Applying a weighted approximation, and introducing a heat flux limiter into the heat flux term $q_{i+\frac{1}{2}}^{n+1}$ presented in equation (7.16),

$$q_{i+\frac{1}{2}}^{n+1} = \left(\theta_1 \cdot q_i^{n+1} + \theta_2 \cdot q_{i+1}^{n+1} + \frac{1}{\lambda}\omega\phi_{i+\frac{1}{2}}^{n+1}(T_{i+1}^{n+1} - T_i^{n+1})\right) \tag{7.19}$$

Where $\phi_{i+\frac{1}{2}}^{n+1}$ is defined as the heat flux limiter, with the following characteristics:

Case I: $T_{i+1}^{n+1} - T_i^{n+1} = 0$,

$$\phi_{i+\frac{1}{2}}^{n+1} = 0 \tag{7.20}$$

Case II: $T_{i+1}^{n+1} - T_i^{n+1} \neq 0$,

$$\phi_{i+\frac{1}{2}}^{n+1} = \lambda\frac{q_{i+1}^n - q_i^n}{T_{i+1}^n - T_i^n} \tag{7.21}$$

and ω is the coefficient of the heat flux limiter, with the constraint

$$0 \leq \omega \leq 1 \tag{7.22}$$

In equation (7.19), θ_1 and θ_2 are weight coefficients with conditions

$$0 < \theta_1 < 1 \quad ; \quad 0 < \theta_2 < 1 \tag{7.23}$$

and

$$\theta_1 + \theta_2 = 1 \tag{7.24}$$

The heat flux term, $q_{i-\frac{1}{2}}^{n+1}$ in equation (7.16), can be similarly transferred through equations (7.19) to (7.24).

Equation (7.16) with the initial condition of equation (7.12), and the boundary conditions at the left hand side ($x = 0$), equations (7.13) and (7.14), cannot be solved directly because the boundary condition at position $x = d$ is unknown. Therefore, an iteration method has to be used. The numerical iteration involves the following four steps:

Step 1: Apply the measured surface temperature and heat flux at $(n+1)\Delta t$ time level, $T_0^{n+1}$and q_0^{n+1}, with the interior temperatures and heat fluxes at the previous $n\Delta t$ time level for mesh $i = 1$ and determine the temporary temperature $\hat{T}_1^{n+1}$by using equation (7.25) as the starting of the iteration process,

$$\hat{T}_1^{n+1} = T_1^n + \lambda \left(\hat{q}_{\frac{3}{2}}^{n+1} - \hat{q}_{\frac{1}{2}}^{n+1} \right) \tag{7.25}$$

where

$$\hat{q}_{\frac{3}{2}}^{n+1} = \left(\theta_1 \cdot \hat{q}_1^{n+1} + \theta_2 \cdot \hat{q}_2^{n+1} + \frac{1}{\lambda} \omega \hat{\phi}_{\frac{3}{2}}^{n+1} (\hat{T}_2^{n+1} - \hat{T}_1^{n+1}) \right) \tag{7.26}$$

$$\hat{q}_{\frac{1}{2}}^{n+1} = \left(\theta_1 \cdot \hat{q}_0^{n+1} + \theta_2 \cdot \hat{q}_1^{n+1} + \frac{1}{\lambda} \omega \hat{\phi}_{\frac{1}{2}}^{n+1} (\hat{T}_1^{n+1} - \hat{T}_0^{n+1}) \right) \tag{7.27}$$

and

$$\hat{\phi}_{\frac{3}{2}}^{n+1} = \begin{cases} 0 & ; \ \hat{T}_2^{n+1} - \hat{T}_1^{n+1} = 0 \\ \lambda \frac{q_2^n - q_1^n}{T_2^n - T_1^n} & ; \ \hat{T}_2^{n+1} - \hat{T}_1^{n+1} \neq 0 \end{cases} \tag{7.28}$$

$$\hat{\phi}_{\frac{1}{2}}^{n+1} = \begin{cases} 0 & ; \ \hat{T}_1^{n+1} - \hat{T}_0^{n+1} = 0 \\ \lambda \frac{q_1^n - q_0^n}{T_1^n - T_0^n} & ; \ \hat{T}_1^{n+1} - \hat{T}_0^{n+1} \neq 0 \end{cases} \tag{7.29}$$

Where $\hat{T}_0^{n+1} = T_0^{n+1}$ and $\hat{q}_0^{n+1} = q_0^{n+1}$ are boundary conditions. As the first iteration cycle, the temporary temperatures $\hat{T}_1^{n+1}$, $\hat{T}_2^{n+1}$ presented in equations (7.26) to (7.29)

and the temporary heat fluxes $\hat{q}_1^{n+1}$, $\hat{q}_2^{n+1}$ presented in equations (7.26) and (7.27) are replaced by the previous recovered values of the temperatures T_1^n , T_2^n , and the heat fluxes q_1^n , q_2^n respectively.

Substituting temporary temperature $\hat{T}_1^{n+1}$ from equation (7.25) into equation (7.15), which gives the corresponding temporary heat flux $\hat{q}_1^{n+1}$,

$$\hat{q}_1^{n+1} = k(T) \cdot \frac{\hat{T}_1^{n+1} - T_0^{n+1}}{\Delta x} \tag{7.30}$$

From this step, we obtain the temporary temperature $\hat{T}_1^{n+1}$ from equation (7.25), and the temporary heat flux $\hat{q}_1^{n+1}$from equation (7.30).

Step 2: Repeat the procedure described in step 1 by using the values of the temporary temperature and temporary heat flux, $\hat{T}_1^{n+1}$and $\hat{q}_1^{n+1}$, to calculate $\hat{T}_2^{n+1}$and $\hat{q}_2^{n+1}$. Then, the procedure is repeated to calculate all the temporary temperatures and the temporary heat fluxes at the mesh points i (*i.e.* $\hat{T}_i^{n+1}$ and $\hat{q}_i^{n+1}$) in the computational domain, to complete the first iteration cycle of the $(n+1)\Delta t$ time level.

Step 3: Apply the measured surface temperature and heat flux at $(n+1)\Delta t$ time level, $T_0^{n+1}$and q_0^{n+1}, with the interior temporary temperatures and temporary heat fluxes from step 1 and 2, and then repeat the procedures of step 1 and 2 again to obtain another set of the temporary temperatures and the temporary heat flux for the second iteration cycle of the $(n+1)\Delta t$ time level.

Step 4: Repeat the procedures of step 3 for the third, fourth, ... and nth

iteration cycles until the difference of the temporary temperatures of the two sequential cycles converge within an allowable small difference. The final convergent temporary temperature $\hat{T}_i^{n+1}$ and the final convergent temporary heat flux $\hat{q}_i^{n+1}$ are the recovered results which represent the temperature T_i^{n+1} and the heat flux q_i^{n+1}, respectively, of $(n+1)\Delta t$ time level.

7.5 Numerical Experiments

An exact solution with the material properties of N-Eicosene paraffin wax is used for the purpose of comparison with the numerical recovered results. The material properties of N-Eicosene paraffin wax are listed as follows:

- Specific heat:

$$\begin{cases} c_s = 2.21 kJ/kg \cdot^\circ C \\ c_l = 2.01 kJ/kg \cdot^\circ C \end{cases}$$

- Density:

$$\begin{cases} \rho_s = 856 kg/m^3 \\ \rho_l = 778 kg/m^3 \end{cases}$$

- Thermal conductivity:

$$\begin{cases} k_s = 1.5002 \times 10^{-4} kJ/m \cdot s \cdot^\circ C \\ k_l = 1.4996 \times 10^{-4} kJ/m \cdot s \cdot^\circ C \end{cases}$$

- Thermal diffusivity:

$$\begin{cases} \alpha_s = 7.93 \times 10^{-8} m^2/s \\ \alpha_l = 9.59 \times 10^{-8} m^2/s \end{cases}$$

- Latent heat: $L = 247kJ/Kg$

- Melting temperature: $T_{melt} = 36.7°C$

The following data are the input for numerical calculation:

- Computational slab length: $d = 5.0cm$

- Initial temperature: $T_i = 25°C$

- Heating surface temperature at $x = 0 : T_o = 60°C$

- Computational mesh size: $\Delta x = 0.1cm$

- Computational time step: $\Delta t = 0.01\,\text{sec}$

- The coefficient of the heat flux limiter $\omega = 0.34$

The exact solutions (Carslaw and Jaeger, 1959) in the liquid and solid regions of the melting problem of a semi-infinite slab placed along an x-axis with the heating surface located at $x = 0$ are as follows:

$$T_l(x,t) = T_o - \frac{(T_o - T_{melt})\text{erf}(\frac{x}{2\sqrt{\alpha_l t}})}{\text{erf}(\eta)}, t > 0, 0 < x < x_{melt}(t) \tag{7.31}$$

$$T_s(x,t) = T_i + \frac{(T_{melt} - T_i)(1 - \text{erf}(\frac{x}{2\sqrt{\alpha_s t}}))}{1 - \text{erf}(\eta\sqrt{\frac{\alpha_l}{\alpha_s}})}, t > 0, x_{melt}(t) < x < d \tag{7.32}$$

where the value of η is determined from the following equation:

$$\frac{e^{-\eta^2}}{\text{erf}(\eta)} - \frac{K_s\sqrt{\alpha_l}(T_i - T_{melt})}{K_l\sqrt{\alpha_s}(T_{melt} - T_o)} \frac{e^{-\alpha_l\eta^2/\alpha_s}}{(1 - \text{erf}(\eta\sqrt{\frac{\alpha_l}{\alpha_s}}))} = \frac{\eta L\sqrt{\pi}}{c_l(T_o - T_{melt})} \tag{7.33}$$

in equations (7.31) to (7.33), $\alpha_l = \frac{k_l}{\rho_l c_l}$ and $\alpha_s = \frac{k_s}{\rho_s c_s}$ are used.

The exact solution of the melting front $x = x_{melt}(t)$ is:

$$x_{melt}(t) = 2\eta\sqrt{\alpha_l t} \tag{7.34}$$

The heat flux at the heating surface $x = 0$ can be obtained from the exact solution equation (7.31) as follows:

$$q_o(t) = q(0,t) = k_l(T)\frac{\partial T_l}{\partial x} \tag{7.35}$$

Figure 7.2 shows the heat flux at the heating surface with the surface temperature $T_o = 60°C$ and initial temperature $T_i = 25°C$. The values of T_o and $q_o(t)$ are used as the known inputs to the above-mentioned inversion solver with the heat flux limiter.

The exact transient temperature distributions at various locations in the liquid and solid regions in the computational domain are shown in Figure 7.3. The recovered temperature distributions, using the weighted coefficients $\theta_1 = 0.95$ and $\theta_2 = 0.05$, with and without heat flux limiter at various locations in the liquid and solid regions in the computational domain, are shown in Figures 7.4 and 7.5, respectively. It is obvious that the heat flux limiter improves the instability phenomena considerably. A comparison of the exact temperature with the recovered temperatures at 2000 sec is shown in Figure 7.6. It can be seen from Figure 7.6 that the recovered temperature obtained without the heat flux limiter oscillates and diverges, while the recovered temperature with the heat flux limiter maintains good stability and is close to the exact solution.

Figure 7.7 shows a comparison between the melting front obtained from the exact solution and those obtained from the inversion solver with different combinations of weighted coefficients (θ_1, θ_2), and the same coefficient $\omega = 0.34$. From this Figure, it can be seen that the recovered melting front obtained from the weighted coefficient $(\theta_1, \theta_2) = (0.7, 0.3)$ is better than that obtained from the weighted coefficients $(0.5, 0.5)$ and $(0.95, 0.05)$ for recovering time less than 1300 sec. For recovering time $1300 \leq t \leq 6000$ sec, the recovered melting front obtained from the weighted coefficients $(\theta_1, \theta_2) = (0.95, 0.05)$ is better than that obtained from the weighted coefficients $(0.5, 0.5)$ or $(0.7, 0.3)$. Figure 7.7 also shows that the recovered melting front diverges away from the exact solution if the heat flux limiter is not used in the recovering procedure. On the other hand, the numerical scheme with the heat flux limiter shortens the computational time. For example, the scheme with the heat flux limiter may use only one-fifth the computational time required for the same scheme without using the heat flux limiter.

7.6 Summary

A semi-explicit time marching finite difference scheme with a heat flux limiter is developed based on the enthalpy formulation of the energy equation, for solving an inverse Stefan problem in one space variable. The advantages of the scheme are summarized as follows:

1. The process may apply to the structure in which sensors are not allowed to be installed inside and/or to maintain structural integrity. For example, in an electric arc furnace, sensors are not able to be installed inside the furnace to measure the melting of the metal skull formed on the inside wall of the furnace.

2. The scheme can handle the phase change problem (Stefan problem) with surface boundary conditions measured at only one side.

3. The scheme developed with the heat flux limiter can stabilize the recovered results of the inverse Stefan problem, and also accelerates rate of convergence.

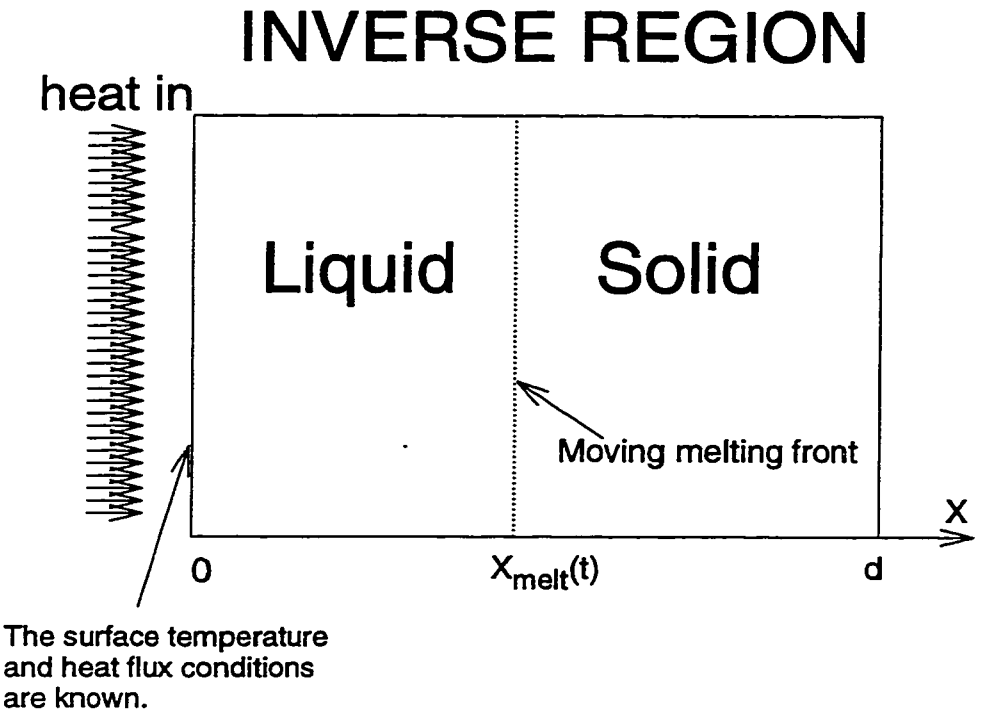

Figure 7.1: Schematic diagram of the inverse Stefan problem

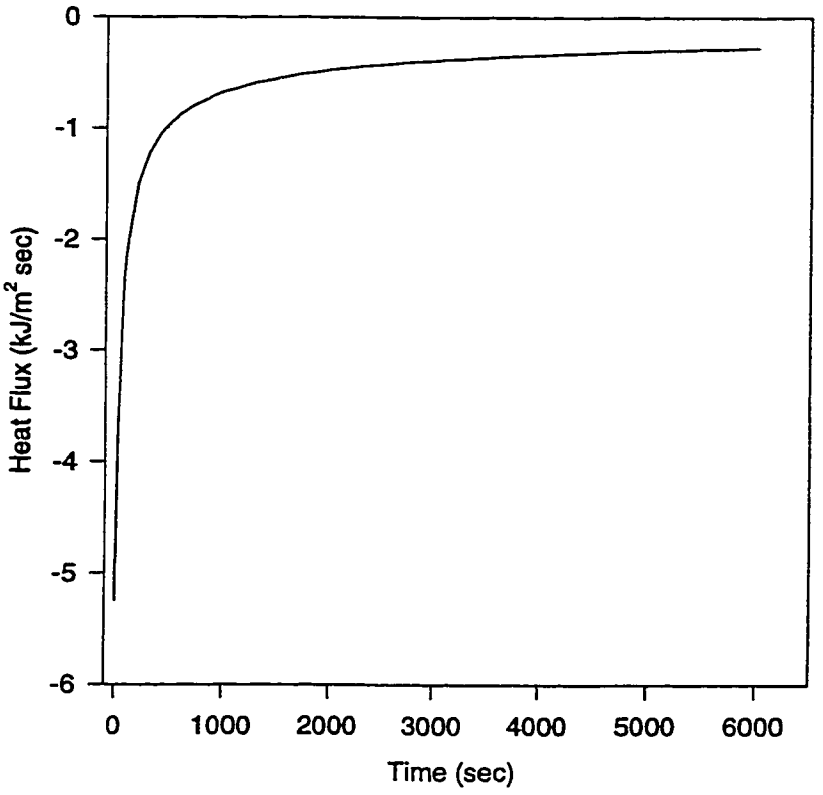

Figure 7.2: The heat flux at the heating surface with the surface temperature $T_o = 60°C$ and initial temperature $T_i = 25°C$.

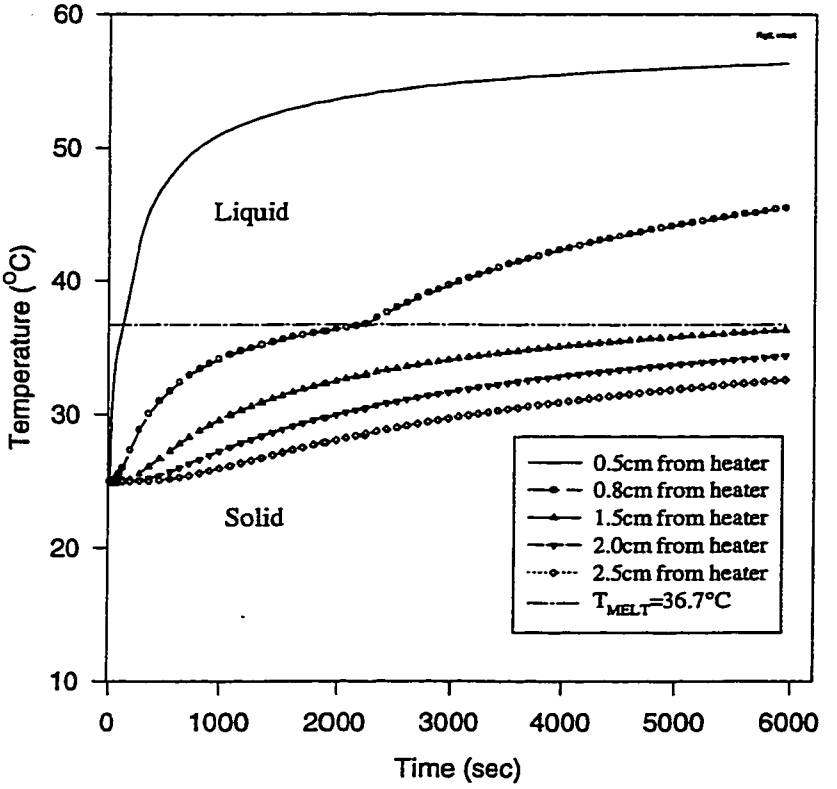

Figure 7.3: The exact solutions of the transient temperature at various locations in the computational domain

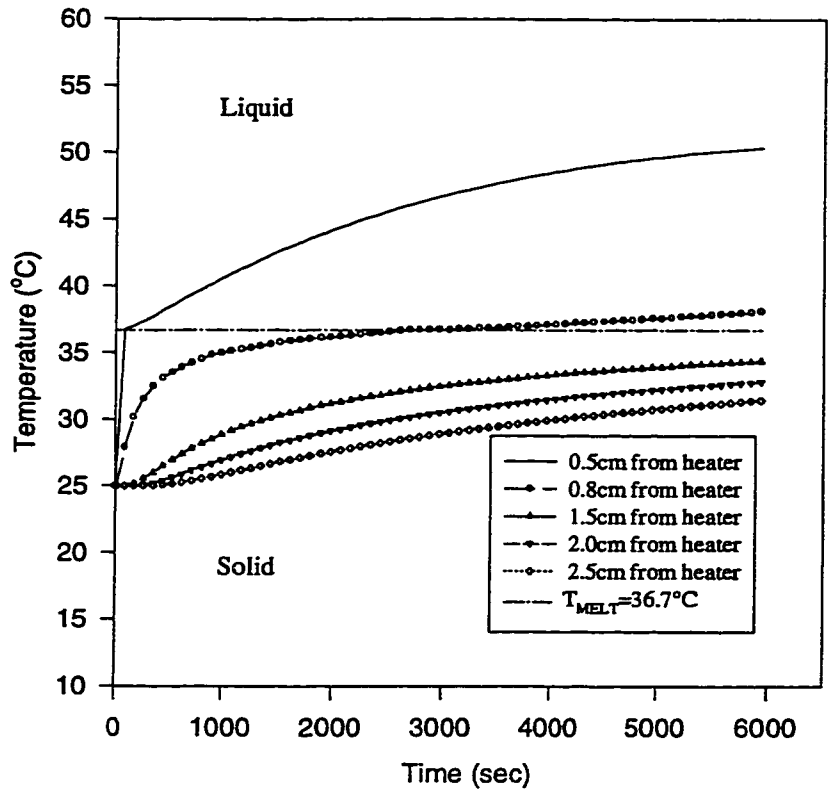

Figure 7.4: The recovered transient temperatures with heat flux limiter at various locations in the computational domain

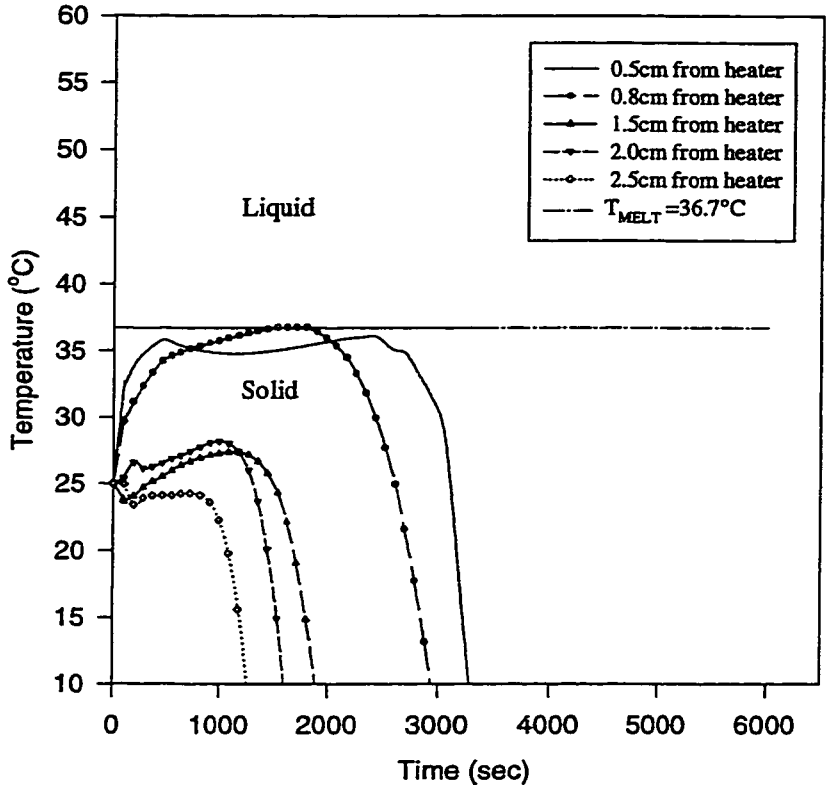

Figure 7.5: The recovered transient temperatures without heat flux limiter at various locations in the computational domain

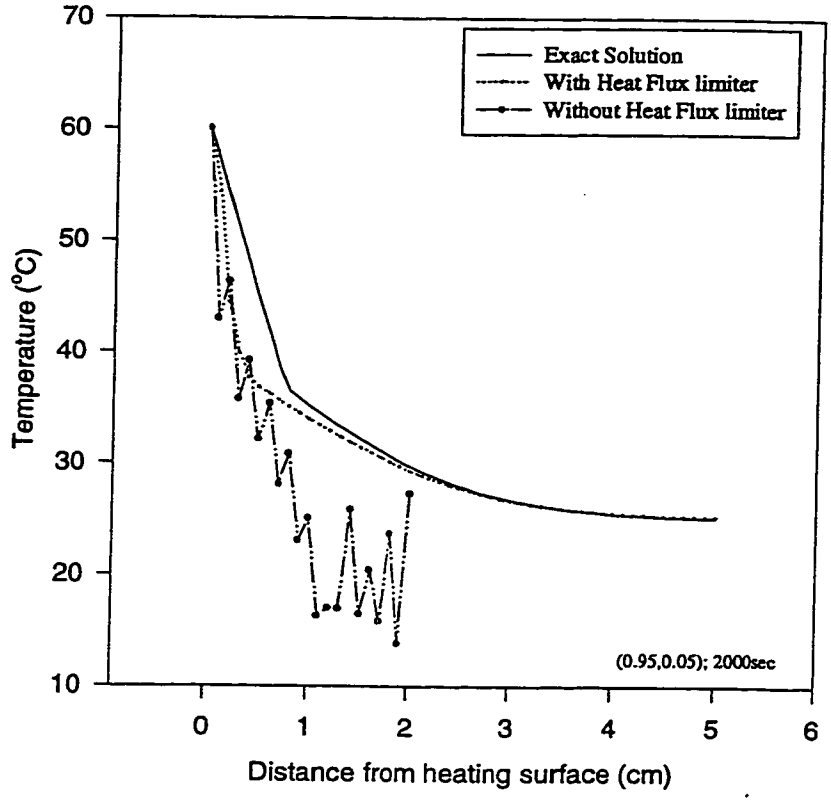

Figure 7.6: Comparison of the recovered temperatures with the exact solution at 2000 sec

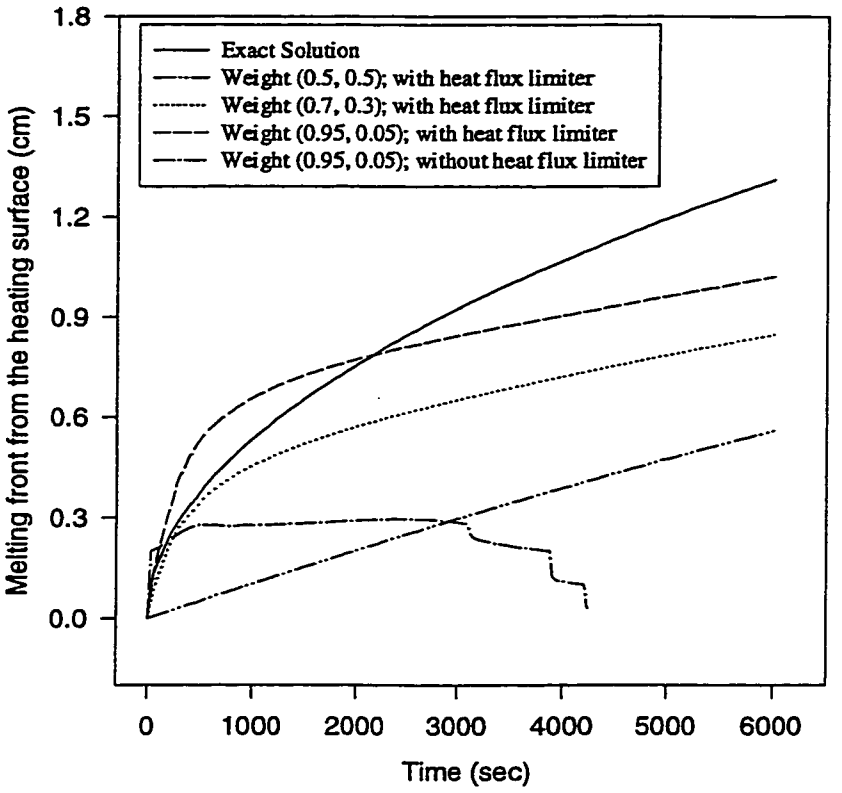

Figure 7.7: Comparison between the melting front obtained from the exact solution and those obtained from the inversion solver with/without heat flux limiter

Chapter 8

Conclusions and Future Work

8.1 Concluding Remarks

Solving an IHCP depends not only on a mathematical model, but also on the stability of the reconstruction results when noisy experimental data are used. With the reconstruction results of the numerical inversion solvers and experimental data presented in this dissertation, the following conclusions and contributions can be established. In Chapters 2 and 3 (Chen, *et al.*, 1996), a new implicit inversion solver for a one-dimensional space IHCP is presented and exhibits good agreement between the exact solution and reconstruction results of the surface temperatures and heat fluxes. The developed inversion solver can also combine with a real-time Kalman Filter. We find that this on-line monitoring inversion solver is very stable in handling noise directly from measurements. Chapter 4 (Chen *et al.*, 1997a), numerical recovery errors of the selected functions, indicates that the errors of the

recovery temperature at both side boundaries and two positions of the interior sensors can be expressed by simple linear relations. Each relation contains an unknown coefficient which can be determined by using one numerical simulation through the inverse solver of a pair of specified sensors. These simple relations, equations (4.1) and (4.2), can then be used to estimate the other recovery errors at the boundary without using the inversion solver. An experimental bench test model (Lin and Chen, 1996, 1997) for comparison with the inversion solver, presented in Chapter 5, has been established. The error between the numerical recovery results and experimental data is small, and has proven that the implicit inversion model is reliable in Chapter 6. One application of the present implicit inversion solver is to determine transient temperature drops due to thermal resistance across two contiguous surfaces between two contact bodies. The present implicit inversion solver can also be extended to reconstruct the temperature distributions in multi-layer composite solids. In Chapter 7 (Chen *et al.*, 1997b), we introduce another new semi-explicit inversion solver by placing the sensors at one side of the surface, which is not limited by the general fact that when two sensors are placed close together, the errors of the recovered temperature and heat flux are increasingly magnified (Hensel, 1991). The recovery temperature profiles and melting front results show that the solution obtained by the semi-explicit inversion solver with the heat flux limiter is much better than those obtained without it.

8.2 Future Work

In order to reconstruct the unknown temperature and heat flux acting on the boundary, or to determine the interior temperature and melting front position through one-sided surface conditions, inversion procedures have to be applied. There are several possible directions in which this dissertation can be extended. The immediate future projects are as follows:

- Use a higher order finite difference approximation, instead of first order, to formulate the unknown left and right hand heat fluxes q_o^{n+1} and q_N^{n+1} at the $(n+1)\Delta t$ time level.
- Apply the real-time Kalman Filter to filter the noise directly from the on-line measurements, and to recover the surface temperatures and heat fluxes.
- Change the heat flux limiter in equation (7.21) to recover an Inverse Stefan problem.
- Optimize the coefficient of the heat flux limiter in equation (7.22).
- Optimize the weighted coefficients θ_1 and θ_2 in equation (7.23).
- Develop a new inversion solver, together with information on average temperature obtained from an ultrasonic sensor, to recover the temperature history inside the conducting body.

Nomenclature

a_1: coefficient of the linear temperature function, equation (4.6)

b_1, b_2: coefficients of the quadratic temperature function, equation (4.7)

c: specific heat, $kJ/Kg \cdot^{\circ} C$

c_1, c_2: coefficients of the exponential temperature function, equation (4.8)

C^A: apparent heat capacity

d: computational slab length, cm

d_1, d_2, ω: coefficients of the periodic temperature function, equation (4.9)

D: partial differential operator

erf$(\cdot)$: error function

$H(T)$: an enthalpy function with temperature variation

k: thermal conductivity, $kJ/m \cdot^{\circ} C \cdot$ sec

l : dimensionless specimen thickness in exact solution

L: latent heat, kJ/Kg

q: heat flux, $kJ/m^2 \cdot \sec$

q_o : heating surface heat flux at $x = 0$ in Chapter 7, $kJ/m^2 \cdot \sec$

$\hat{q}$: temporary heat flux at $(n+1)\Delta t$ time level, $kJ/m^2 \cdot \sec$

S_- : backward shift operator

S_+ : forward shift operator

t : dimensionless time variable in Chapters 2-6, and time variable in Chapter 7, *sec*

T : dimensionless temperature variable in Chapters 2-6, and temperature variable in Chapter 7, $°C$

$\hat{T}$: temporary temperature at $(n+1)\Delta t$ time level, $°C$

T_i : initial temperature, $°C$

T_o : heating surface temperature at $x = 0$ in Chapter 7, $°C$

Δt : time mesh size of finite difference scheme

U : correlation matrix for $n\Delta t$ and $(n+1)\Delta t$ time levels

$\underline{v}$: additive white noise

χ_L: left hand sensor location in dimensionless space

χ_L^* : left hand specified sensor location

χ_M: right hand sensor location in dimensionless space

χ_M^* : right hand specified sensor location

χ_N: right hand specified boundary in dimensionless space

Δx : space mesh size of finite difference scheme

x : dimensionless space variable in x direction in Chapters 2-6, and space variable in x direction in Chapter 7, m

Δx : dimensionless space mesh size in x direction in Chapters 2-6, and space mesh size in x direction in Chapter 7, m

$\underline{y}$: measured vector

$\underline{z}$: state vector

$\hat{\underline{z}}$: linear estimate from Kalman Filter

Greek symbols:

ϵ: a very small number, $\epsilon = 0.1°C$ in Chapter 7

ω: heat flux limiter coefficient

θ_1, θ_2: weighted coefficients

ϕ: heat flux limiter function

$\hat{\phi}$: temporary heat flux limiter function at $(n+1)\Delta t$ time level

α: diffusivity, $m^2/\sec$

Γ: temperature integration variable, $°C$

ρ: density, Kg/m^3

$\delta(\cdot)$: Dirac function

λ : $\frac{\Delta t}{(\Delta x)^2}$ in Chapter 2, and $\frac{1}{C^A(T)}\ \frac{\Delta t}{\Delta x}$ in Chapter 7

Ω: a bounded region

$\partial\Omega$: the boundary of a bounded region

σ_{LH}: error of the reconstruction temperature at the left hand boundary; %

σ^*_{LH}: error of the reconstruction temperature at the left hand boundary with two specified sensor locations; %

σ_{RH}: error of the reconstruction temperature at the right hand boundary; %

σ^*_{RH}: error of the reconstruction temperature at the right hand boundary with two specified sensor locations; %

Λ_{LH}: constant coefficient for simple relation at the left hand boundary

Λ_{RH}: constant coefficient for simple relation at the right hand boundary

subscripts:

i : mesh point location in x direction

l : liquid phase

L: mesh point of left hand sensor location in finite difference scheme

$melt$: melting front

M: mesh point of right hand sensor location in finite difference scheme

N: mesh point of right hand specified boundary in finite difference scheme

o: mesh point of left hand boundary in finite difference scheme

s : solid phase

superscript:

n : time level

Bibliography

[1] Alexandrou, Andreas N., An Inverse Finite Element Method for Directly Formulated Free Boundary Problems, *International Journal for Numerical Methods in Engineering*, vol. **28**, pp. 2383-2396 (1989).

[2] Alexandrou, Andreas N., Elden, Robert and McConnell, Jeff, An Inverse Approach to Three-Dimensional Solidification Problems, *International Journal for Numerical Methods in Engineering*, vol. **36**, pp. 135-145 (1993).

[3] Alifanov, Oleg M., Inverse Boundary-Value Problems of Heat Conduction, *Journal of Engineering Physics, vol.* **29(1)**, pp. 821-830 (1975).

[4] Alifanov, Oleg M., Inverse Heat Transfer Problems, Springer-Verlag, Berlin (1994).

[5] Beck, James V., Nonlinear Estimation Applied to the Nonlinear Inverse Heat Conduction Problem, *Int. J. Heat Mass Transfer*, vol. **13**, pp. 703-715 (1970).

[6] Beck, James V., Blackwell, Ben and St. Clair, C. R. Jr., Inverse heat Conduction, John Wiley & Sons, Inc., New York (1985).

[7] Bénard, C., Gobin D. and Zanoli, A., Moving Boundary Problem: Heat Conduction in the Solid Phase of a Phase-Change Material During Melting Driven by Natural Convection in the Liquid, *Int. J. Heat Mass Transfer*, vol. **29**, pp. 1669-1681 (1986).

[8] Bénard, C. and Afshari, A., Inverse Stefan Problem: Tracking of the interface position from measurements on the solid phase, *International Journal for Numerical Methods in Engineering*, vol. **35**, pp. 835-851 (1992).

[9] Bennon, W. D. and Incropera, F. P., A Continuum Model for Momentum, Heat and Species Transport in Binary Solid-Liquid Phase Chang System–I. Model Formulation, *Int. J. Heat Mass Transfer*, vol. **30**, pp. 2161-2170 (1987).

[10] Bonacina, C., Comini, G., Fasano, A and Primicerio, M., Numerical Solution of Phase Change Problems, *Int. J. Heat Mass Transfer*, vol. **16**, pp. 1825-1832 (1973).

[11] Burggraf, O. R., An Exact Solution of the Inverse Problem in Heat Conduction Theory and Application, *ASME J. Heat Transfer*, vol. **86**, pp. 373-382 (1964).

[12] Carslaw, H. S. and Jaeger, J. C., Conduction of Heat in Solids, Oxford University Press, Oxford, U.K. (1959).

[13] Celia, Michael A. and Gray, William G., Numerical Methods for Differential Equations, Prentice-Hall, Inc., New Jersey (1992).

[14] Chen, T. F., Lin, S., and Wang, J. C. Y., Kalman Filter and Finite Difference Scheme to Inverse Heat Conduction Problems, *Inverse Problems in Engineering*, vol. **3**, pp. 162-175 (1996).

[15] Chen, T. F., Lin, S., and Wang, J. C. Y., Determination of Boundary Temperature Errors by Variation of Two Temperature Sensor Locations in One-Dimensional Inverse Heat Conduction Problem, to appear in *International Journal of Numerical Methods for Heat and Fluid Flow* (1997a).

[16] Chen, T. F., Lin, S., Wang, J. C. Y., and Chen, T. J., A Heat Flux Limiter Finite Difference Scheme in Solving a One-Dimensional Inverse Stefan Problem, to appear in *Inverse Problems in Engineering* (1997b).

[17] Civan, Faruk and Sliepcevich, C. M., Efficient Numerical Solution for Enthalpy Formulation of Conduction Heat Transfer with Phase Change, *Int. J. Heat Mass Transfer*, vol. **27**, pp. 1428-1430 (1984).

[18] Clausing, A. M., and Chao, B. T., Thermal Contact Resistance in a Vacuum Environment, *ASME J. Heat Transfer*, vol. **87**, pp. 243-251 (1965).

[19] Colton, David and Reemtsen, Rembert, The Numerical Solution on the Inverse Stefan Problem in Two Space Variables, *SIAM J. Appl. Math.*, vol. **44**, pp. 996-1013 (1984).

[20] Crank, John, How to Deal with Moving Boundaries in Thermal Problems, Numerical Methods in Heat Transfer edited by Lewis, R. W. *et al.,* John Wiley & Sons Ltd., New York, pp. 177-200 (1981).

[21] Crank, John, Free and Moving Boundary Problems, Clarendon Press, Oxford (1984).

[22] Dantzig, Jonathan A., Modelling Liquid-Solid Phase Changes with Melt Convection, *International Journal for Numerical Methods in Engineering*, vol. **28**, pp. 1769-1785 (1989).

[23] Date, A. W., A Strong Enthalpy Formulation for Stefan Problem, *Int. J. Heat Mass Transfer*, vol. **34**, pp. 2231-2235 (1991).

[24] Deverall, L. I. and Channapragada, R. S., A New Integral Equation for Heat Flux in Inverse Heat Conduction, *ASME J. Heat Transfer*, vol. **88**, pp. 327-328 (1966).

[25] Dursunkaya, Z. and Nair, S., A Moving Boundary Problem in a Finite Domain, *ASME J. Applied Mechanics*, vol. **57**, pp. 50-56 (1990).

[26] El-Genk, Mohamed S. and Cronenberg, August W., Some Improvements to the Solution of Stefan-Like Problems, *Int. J. Heat Mass Transfer*, vol. **22**, pp. 167-170 (1979).

[27] Faires, V. M., Thermodynamics, 6th edition, Macmillan Publishing Co., Inc., New York (1978).

[28] Flach, G. P. and Özişik, M. N., Inverse Heat Conduction Problem of Simultaneously Estimating Spatially Varying Thermal Conductivity and Heat Capacity per Unit Volume, *Numer. Heat Transfer*, Part A, vol. **16**, pp. 441-461 (1989).

[29] Flach, G. P. and Özişik, M. N., An Adaptive Inverse Heat Conduction Method with Automatic Control, *ASME J. Heat Transfer*, vol. **114**, pp. 5-13 (1992).

[30] Forslund, R. P. and Oliveira, H. Q., Thermal effect of thermal constriction resistance in the design of channel plate heat exchanger: Cylindrical geometry, *ASME J. Heat Transfer*, vol. **97**, pp. 619-621 (1975).

[31] Frank, I., An Application of Least Squares Method to the Solution of the Inverse Problem of Heat Conduction, *ASME J. Heat Transfer*, vol. **85**, pp. 378-379 (1963).

[32] Garabedian, P. R., Partial Differential Equations, John Wiley & Sons, Inc., New York (1964).

[33] Grange, B. W., Viskanta, R. and Stevenson, W. H., Diffusion of Heat and Solute During Freezing of Salt Solutions, *Int. J. Heat Mass Transfer*, vol. **19**, pp. 373-384 (1976).

[34] Hadamard, Jacques, Lectures on Cauchy's Problem in Linear Partial Differential Equations, Yale University Press (1923).

[35] Hastaoglu, Mehmet A., A Numerical Solution to Moving Boundary Problems – Application to Melting and Solidation, *Int. J. Heat Mass Transfer*, vol. **29**, pp. 495-499 (1986).

[36] Heinrich, J. C., Felicelli, S. and Poirier, D. R., Vertical Solidification of Dendritic Binary Alloys, *Computer Methods in Applied Mechanics and Engineering*, vol. **89**, pp. 435-461 (1991).

[37] Hensel, E., Inverse Theory and Applications for Engineers, Prentice Hall, New Jersey (1991).

[38] Hills, R. G. and Hensel, E. C., Jr., One-Dimensional Nonlinear Inverse Heat Conduction Technique, *Numer. Heat Transfer*, vol. **10**, pp. 369-393 (1986).

[39] Hills, R., Raynaud, M., and Hensel, E., Surface Variance Estimates Using an Adjoint Formulation for a One Dimensional Nonlinear Inverse Heat Conduction Technique, *Numer. Heat Transfer*, vol. **10**, pp. 441-461 (1986).

[40] Hsieh, C. K., Exact Solutions of Stefan Problems for a Heat Front Moving at Constant Velocity in a Quasi-steady State, *Int. J. Heat Mass Transfer*, vol. **38**, pp. 71-79 (1995).

[41] Hsu, C. F., Sparrow, E. M. and Patankar, S. V., Numerical Solution of Moving Boundary Problems by Boundary Immobilization and a Control-Volume-Based Finite-Difference Scheme, *Int. J. Heat Mass Transfer*, vol. **24**, pp. 1335-1343 (1981).

[42] Hsu, T. R., Sun, N. S., Chen, G. G. and Gong, Z. L., Finite Element Formulation for Two-Dimensional Inverse Heat Conduction Analysis, *ASME J. Heat Transfer*, vol. **114**, pp. 553-557 (1992).

[43] Isaac Shai and Mordechai Santa, "Heat Transfer with Contact Resistance", *Int. J. Heat Mass Transfer*, vol. **25**, pp. 465-470 (1982).

[44] Kang, B., Zhao, Z. and Poulikakos, D., Solidification of Liquid Metal Droplets Impacting Sequentially on a Solid Surface, *ASME J. Heat Transfer*, vol. **116**, pp. 436-445 (1994).

[45] Kang, Shinill and Zabaras, Nicholas, Control of the Freezing Interface Motion in Two-Dimensional Solidification Processes Using the Adjoint Method, *International Journal for Numerical Methods in Engineering*, vol. **38**, pp. 63-80 (1995).

[46] Katz, Michael A. and Rubinsky, Boris, An Inverse Finite Element Technique to Determine the Change of Phase Interface Location in One-Dimensional Melting Problems, *Numerical Heat Transfer*, vol. **7**, pp. 269-283 (1984).

[47] Kececioglu, Ifiyenia and Rubinsky, Boris, A Continuum Model for the Propagation of Discrete Phase-Change Fronts in Porous Media in the Presence of Coupled Heat Flow, Fluid Flow and Species Transport Processes, *Int. J. Heat Mass Transfer*, vol. **32**, pp. 1111-1130 (1989).

[48] Kilingenberg, C. and Mao, D.-K., The Total Variation Decreasing Property of a Conservation Front Tracking Technique, *Mathl. Comput. Modelling*, vol. **20**, pp. 89-99 (1994).

[49] Kreith, Frank and Bohn, Mark S., Principles of Heat Transfer, Harper & Row, Publisher, Inc., New York (1986).

[50] Kurpisz, K., Numerical Solution of One Case of Inverse Heat Conduction Problems, *ASME J. Heat Transfer*, vol. **113**, pp. 280-286 (1991).

[51] Lamm, Patricia K., Inverse Problems and Ill-posedness, *ASME Inverse Problems in Engineering: Theory and Practice,* pp. 1-10 (1993).

[52] Lee, S. L. and Tzong, R. Y., Latent Heat Method for Solidification Process of a Binary Alloy System, *Int. J. Heat Mass Transfer*, vol. **38**, pp. 1237-1247 (1995).

[53] Lin, Sui, An Estimation of the Thickness of Metal Skull Formed on a Wall of an Electric Arc Furnace, *ASME Inverse Problems in Engineering: Theory and Practice*, pp. 343-347 (1993).

[54] Lin, S., Chen, T. F. and Chen, D. K., Drying Process in a Porous Medium with a Non-Penetrating Heating Surface, *International Conference on Porous Media and Its Application in Science, Engineering and Industry*, Hawaii., pp. 199-212 (1996).

[55] Lin, S., Chao, J. T., Chen, T. F. and Chen, D. K., An Analytical and Experimental Study of Drying Process in a Porous Medium with a Non-Penetrating Heating Surface, to appear in *Journal of Porous Media* (1997).

[56] Lunardini, V. J., Phase Change Around Insulated Buried Pipes: Quasi-Steady Method, *ASME J. Energy Resources Technology*, vol. **103**, pp. 201-207 (1981).

[57] Lunardini, V. J., Heat Transfer in Cold Climates, Van Nostrand Reinhold Company, New York (1981).

[58] Maillet, D., A. Degiovanni and R. Pasquetti, Inverse Heat Conduction Applied to the Measurement of Heat Transfer Coefficients on a Cylinder: Comparison Between an Analytical and a Boundary Element Technique, *ASME J. Heat Transfer*, vol. **113**, pp. 549-557 (1991).

[59] Mashena, M. and Haji-Sheikh, A., An Integral Solution of Moving Boundary Problems, *Int. J. Heat Mass Transfer*, vol. **29**, pp. 317-329 (1986).

[60] McDaniel, David and Zabaras, Nicholas, A Least-Squares Front-Tracking Finite Element Method Analysis of Phase Change with Natural Convection, *International Journal for Numerical Methods in Engineering*, vol. **37**, pp. 2755-2777 (1994).

[61] Mikic, B. B., Thermal Contact Resistance Due to Non-uniform Surface Conditions, Contact Resistance at Non-uniform Interface Pressure, *Int. J. Heat Mass Transfer*, vol. **13**, pp. 1497-1500 (1970).

[62] Miranda, C., Partial Differential Equations of Elliptic Type, 2nd Edition, (Original version written in Russian, 1954), Springer-Verlag, Berlin (1970).

[63] Mori , A. and Araki, K., Methods for Analysis of the Moving Boundary-Surface Problem, *International Chemical Engineering*, vol. **16**, pp. 734-743, (1976).

[64] Murio, Diego A., The Mollification Method and Numerical Solution of Ill-posed Problems, John Wiley & Sons, Inc., New York (1993).

[65] Murio, Diego A., On the Numerical Solution of the Two-Dimensional Inverse Heat Conduction Problem by Discrete Mollification, *ASME Inverse Problems in Engineering: Theory and Practice*, pp. 17-21 (1993).

[66] Myint-U, T., Partial Differential Equations of Mathematical Physics, American Elsevier Publishing Company, Inc., New York (1973).

[67] Nashed, M. Zuhair, Editor, Generalized Inverses and Applications, Academic Press, New York (1976).

[68] Neto, A. J. Silva and Özişik M. N., Inverse Problem of Simultaneously Estimating the Timewise-Varing Strengths of Two Plane Heat Sources, *J. Appl. Phys*, vol. **73**, pp. 2132-2137, (1993).

[69] Neto, A. J. and White, R. E., Numerical Control of the Stefan Problem: Maximum Melting, *Computer Methods in Applied Mechanics and Engineering*, vol. **113**, pp. 351-362 (1994).

[70] Norton, S. J., Simmons, J. A., Kahn, A. H. and Wadley, H. N. G., Research on Inverse Problems in Materials Science and Engineering, Signal Processing and Pattern Recognition in Nondestructive Evaluation of Materials, edited by Chen, C. H., Springer-Verlag, Berlin, NATO ASI Series, vol. **F44**, pp.1-21 (1988).

[71] Özişik, M. N., Basic Heat Transfer, McGraw-Hill Book Company, New York (1977).

[72] Payne, L. E., On Stabilizing Ill-Posed Cauchy Problems for the Navier-Stokes Equations, Differential Equations with Applications to Mathematical Physis, Academic Press, Inc., Boston, pp. 261-271 (1993).

[73] Payne, L. E., Improperly Posed Problems in Partial Differential Equations, Society for Industrial and Applied Mathematics, Philadelphia (1975).

[74] Prescott, P. J. and Incropera, F. P., Modeling of Dendritic Solidification Systems: Reassessment of the Continuum Momentum Equation, *Int. J. Heat Mass Transfer*, vol. **34**, pp. 2351-2359 (1991).

[75] Rabin, Y. and Shitzer, A., Exact Solution to the One-Dimensional Inverse-Stefan Problem in Nonideal Biological Tissues, *ASME J. Heat Transfer*, vol. **117**, pp. 425-431 (1995).

[76] Randall, John D., Finite Difference Solution of the Inverse Heat Conduction Problem and Ablation, *The Johns Hopkins University Applied Physics Laboratory, Laurel, Md. 20810* (1976).

[77] Raynaud, M. and Bransier, J., A New Finite Difference Method for the Nonlinear Inverse Heat Conduction Problem, *Numer. Heat Transfer*, vol. **9**, pp. 27-42 (1986).

[78] Reinhardt, H.-J., A Numerical Method for the Solution of Two-Dimensional Inverse Heat Conduction Problems, *International Journal for Numerical Methods in Engineering*, vol. **32**, pp. 363-383 (1991).

[79] Ruan, Y., Liu, J. C. and Richmond, O., Determining the Unknown Cooling Condition and Contact Heat Transfer Coefficient During Solidification of Alloys, *Inverse Problems in Engineering*, vol. **1**, pp. 45-69 (1994).

[80] Rubinsky, Boris and Cravahlo, Ernest G., A Finite Element Method for the Solution of One-Dimensional Phase Change Problems, *Int. J. Heat Mass Transfer*, vol. **24**, pp. 1987-1989 (1981).

[81] Saitoh, T. S., Nakamura, M. and Gomi, T., Time-Space Method for Multidimensional Melting and Freezing Problems, *International Journal for Numerical Methods in Engineering*, vol. **37**, pp. 1793-1805 (1994).

[82] Savateev, E. G. and Riganti, R., Inverse Problem for Nonlinear Heat Equation with the Final Overdetermination, *Mathl. Comput. Modelling*, vol. **22**, pp. 29-43 (1995).

[83] Sawaf, B and Özişik, M. N., An Inverse Analysis to Estimate Linearly Temperature Dependent Thermal Conductivity Components and Heat Capacity of an Orthotropic Medium, *Int. J. Heat Mass Transfer*, vol. **38**, pp. 3005-3010 (1995).

[84] Scarpa, F. and Milano, G., Kalman Smoothing Technique Applied to the Inverse Heat Conduction Problem, *Numer. Heat Transfer, Part B*, vol. **28**, pp. 79-96 (1995).

[85] Shai, I. and Santa M., Heat transfer with contact resistance, *Int. J. Heat Mass Transfer*, vol. **25**, pp. 465-470 (1982).

[86] Shamsundar, N. and Sparrow, E. M., Effect of Density Change on Multidimensional Conduction Phase Change, *ASME J. Heat Transfer*, vol. **98**, pp. 550-557 (1976).

[87] Shamsundar, N. and Sparrow, E. M., Analysis of Multidimensional Conduction Phase Change *Via* the Enthalpy Model, *ASME J. Heat Transfer*, vol. **97**, pp. 333-340 (1975).

[88] Shau, R., Batista, J. and Carey, G. F., An Improved Algorithm for Inverse Design of Thermal Problems With Multiple Materials, *ASME J. Heat Transfer*, vol. **112**, pp. 274-279 (1990).

[89] Shyy, Wei and Chen, M.-H., Steady-State Natural Convection with Phase Change, *Int. J. Heat Mass Transfer*, vol. **33**, pp. 2545-2563 (1990).

[90] Sorenson, H. W., Kalman Filtering Techniques, *Advances in Control Systems Theory and Applications*, vol. **3**, pp. 219-292 (1966).

[91] Sparrow, E. M., Haji-Sheikh, A and Lundgren T. S., The Inverse Problem in Transient Heat Conduction, *ASME J. Applied Mechanics*, September, pp. 369-375 (1964).

[92] Stolz G., Jr., Numerical Solutions to an Inverse Problem of Heat Conduction for Simple Shapes, *ASME J. Heat Transfer*, vol. **82**, pp. 20-26 (1960).

[93] Street, Robert L., The Analysis and Solution of Partial Differential Equations, Brooks/Cole Publishing Company, Monterey, Calif. (1973).

[94] Tezduyar, T. E., Behr, M. and Liou, J., A New Strategy for Finite Element Computations Involving Moving Boundaries and Interfaces – The Deforming-Spatial-Domain / Space-time Procedure: I. The Concept and the Preliminary Numerical Test, *Computer Methods in Applied Mechanics and Engineering*, vol. **94**, pp. 339-351 (1992).

[95] Tezduyar, T. E., Behr, M. and Liou, J., A New Strategy for Finite Element Computations Involving Moving Boundaries and Interfaces – The Deforming-Spatial-Domain / Space-time Procedure: II. Computation of Free-Surface Flows, Two-Liquid Flows, and Flows with Drifting Cylinders, *Computer Methods in Applied Mechanics and Engineering*, vol. **94**, pp. 353-371 (1992).

[96] Thomas, T. R., Extrapolation Errors in Thermal Contact Resistance Measurements, *ASME J. Heat Transfer*, vol. **96**, pp. 305-307 (1975).

[97] Tikhonov, Andrey N., and Arsenin, Vasiliy Y., Solutions of Ill-posed Problems, V. H. Winston & Sons, Washington, D.C. (1977).

[98] Veillette, P., Thermal Conductivity of Richards Bay Ore, Report No. R-34-92, QIT-Fer et Titane Inc., Sorel, Québec (1992).

[99] Viskanta R., Heat Transfer During Melting and Solidification of Metals, *ASME J. Heat Transfer*, vol. **110**, pp. 1205-1219 (1988).

[100] Voller, V. R. and Cross, M., Estimating the Solidification/Melting Times of Cylindrically Symmetric Regions, *Int. J. Heat Mass Transfer*, vol. **24**, pp. 1457-1462, (1981a).

[101] Voller, V. R. and Cross, M., Accurate Solutions of Moving Boundary Problems Using the Enthalpy Method, *Int. J. Heat Mass Transfer*, vol. **24**, pp. 545-556 (1981b).

[102] Voller, V. R. and Cross, M., An Explicit Numerical Method to Track a Moving Phase Change Front, *Int. J. Heat Mass Transfer*, vol. **26**, pp. 147-150 (1983).

[103] Voller, V. R., A Heat Balance Integral Method Based on an Enthalpy Formulation, *Int. J. Heat Mass Transfer*, vol. **30**, pp. 604-607 (1987).

[104] Voller, V. R. and Prakash, C., A Fixed Grid Numerical Modelling Methodology for Convection-Diffusion Mushy Region Phase-Change Problems, *Int. J. Heat Mass Transfer*, vol. **30**, pp. 1709-1719 (1987).

[105] Voller, V. R. and Brent, A. D., The Modelling of Heat, Mass and Solute Transport in Solidification Systems, *Int. J. Heat Mass Transfer*, vol. **32**, pp. 1719-1731 (1989).

[106] Voller, V. R. and Swaminathan, C. R., Fixed Grid Techniques for Phase Change Problems : A Review, *International Journal for Numerical Methods in Engineering*, vol. **30**, pp. 875-898 (1990).

[107] Wang, J. C. Y., Thermal Constriction Resistance in Cylindrical Surfaces, Ph. D. dissertation, Faculty of Engineering Science, University of Western Ontario, London, Canada (1981).

[108] Weinberger, H. F., Partial Differential Equations with Complex Variables and Transform Methods, Blaisdell Publishing Co., Waltham, Mass. (1965).

[109] Yao, L. S., Prusa, J., Melting and Freezing, *Advances in Heat Transfer,* Academic Press, Inc., vol. **19**, pp. 1-95 (1989).

[110] Yao, Minwu and Chait, Arnon, A Conservative Formulation of the Apparent Heat Capacity Method for Heat Transport Problems with Phase Change, *The 6th International Symposium on Transport Phenomena in Thermal Engineering, Seoul, Korea*, pp. 41-46 (1993).

[111] Yovanovich, M. M., Burde, S. S. and Thompson, J. C., Thermal Constriction Resistance of Arbitrary Planar Contact with Constant Flux, *AIAA 11th Thermophysics Conference* (1976).

[112] Yuen, W.W., Application of the Heat-Balance Integral to Melting Problems with Initial Subcooling, *Int. J. Heat Mass Transfer*, vol. **23**, pp. 1157-1160 (1980).

[113] Zabaras, Nicholas and Liu, Joshua C., An Analysis of Two-Dimensional Linear Inverse Heat Transfer Problems Using an Integral Method, *Numerical Heat Transfer*, vol. **13**, pp. 527-533 (1988).

[114] Zabaras, Nicholas, Inverse Finite Element Techniques for the Analysis of Solidification Processes, *International Journal for Numerical Methods in Engineering*, vol. **29**, pp. 1569-1587 (1990).

[115] Zabaras, Nicholas and Kang, Shinill, On the Solution of an Ill-posed Design Solidification Problem Using Minimization Techniques in Finite- and Infinite-Dimensional Function Spaces, *International Journal for Numerical in Engineering*, vol. **36**, pp. 3973-3990 (1993).

[116] Zachmanoglou, E. C. and Thoe, D. W., Introduction to Partial Differential Equations with Application, The Williams & Wilkins Co., Baltimore (1975).

Appendix A

Inversion model I for Inversion Heat Conduction Problems

Inversion Heat Conduction Problems: the temperature at position $x = \chi_M$, T_M (measured temperature), and the heat flux at position $x = \chi_N$, q_N, as shown on figure A.1, are known. Matrix U of equation(2.12) is represented by:

$$U = \begin{bmatrix} 1+\lambda & -\lambda & 0 & \cdots & 0 & 0 & \lambda\Delta x & 0 & 0 & \cdots & & & 0 \\ -\lambda & 1+2\lambda & -\lambda & & & & 0 & & & & & & \\ & & & & \cdot & \cdot & \cdot & & & & & & \\ & & & -\lambda & 1+2\lambda & -\lambda & \cdot & & & & & & \\ & & & & -\lambda & 1+2\lambda & 0 & & & & & & \\ & & & & & -\lambda & 0 & -\lambda & & & & & \\ & & & & & & 0 & 1+2\lambda & -\lambda & & & & \\ & & & & & & \cdot & -\lambda & 1+2\lambda & -\lambda & & & \\ & & & & & & \cdot & & \cdot & \cdot & \cdot & & \\ & & & & & & & & \cdot & \cdot & -\lambda & 1+2\lambda & -\lambda \\ 0 & & & & & & 0 & & & \cdots & & -\lambda & 1+\lambda \end{bmatrix} \quad \text{(A.1)}$$

The unknown matrix $\underline{T}^{n+1}$ of equation (2.12) is:

$$\underline{T}^{n+1} = \begin{bmatrix} T_1^{n+1} \\ . \\ . \\ . \\ T_{M-1}^{n+1} \\ q_1^{n+1} \\ T_{M+1}^{n+1} \\ . \\ . \\ . \\ T_N^{n+1} \end{bmatrix} \tag{A.2}$$

The matrix $\underline{T}^n$ of equation (2.12) is:

$$\underline{B}^n = \begin{bmatrix} T_1^n \\ . \\ . \\ . \\ T_{M-1}^n + \lambda T_M^{n+1} \\ T_M^n - (2\lambda + 1) T_M^{n+1} \\ T_{M+1}^n + \lambda T_M^{n+1} \\ . \\ . \\ . \\ T_N^n + \lambda \Delta x q_N^{n+1} \end{bmatrix} \tag{A.3}$$

Because at position $x = \chi_M$, the temperature ${T_M}^{n+1}$ is known, by applying the left hand side unknown boundary condition ${q_1}^{n+1}$, we can substitute ${q_1}^{n+1}$ (the heat flux at the left boundary $x = 0$ as shown on figure A.1) into the left side $\underline{T}^{n+1}$ matrix.

Then, the unknown elements of the matrix $\underline{T}^{n+1}$ can be solved by the time-marching scheme.

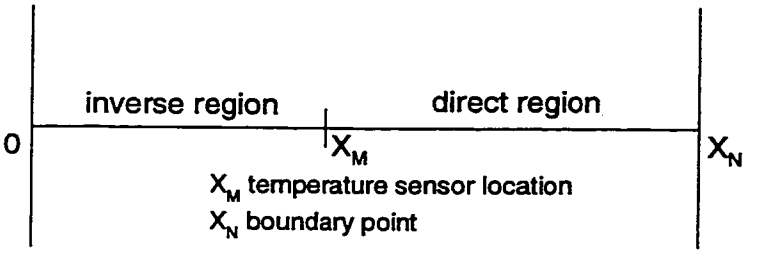

Unknown conditions:
$Q(0,t) = ?$
$T(0,t) = ?$

Known conditions:
$Q(X_N,t)$ = Known heat flux at X_N
$T(X_M,t)$ = Known temperature at X_M

Figure A.1: One-dimensional inverse heat conduction problem: model I

Appendix B

Inversion model II for Inversion Heat Conduction Problems

The temperatures at the measurement position $x = \chi_M$ and boundary position $x = \chi_N$ (as shown on figure B.1), are known from the measured values. Matrix U of equation (2.12) is:

$$U = \begin{bmatrix} 1+\lambda & -\lambda & 0 & \cdots & 0 & 0 & \lambda\Delta x & 0 & 0 & \cdots & & & 0 \\ -\lambda & 1+2\lambda & -\lambda & & & & 0 & & & & & & \\ & & & & \cdot & \cdot & \cdot & & & & & & \\ & & & -\lambda & 1+2\lambda & -\lambda & \cdot & & & & & & \\ & & & & -\lambda & 1+2\lambda & 0 & & & & & & \\ & & & & & -\lambda & 0 & -\lambda & & & & & \\ & & & & & & 0 & 1+2\lambda & -\lambda & & & & \\ & & & & & & \cdot & -\lambda & 1+2\lambda & -\lambda & & & \\ & & & & & & \cdot & & \cdot & \cdot & \cdot & & \\ & & & & & & & & \cdot & \cdot & -\lambda & 1+2\lambda & -\lambda \\ 0 & & & & & & 0 & & & \cdots & & -\lambda & 1+2\lambda \end{bmatrix} \quad \text{(B.1)}$$

The unknown matrix $\underline{T}^{n+1}$ of equation (2.12) is:

$$\underline{T}^{n+1} = \begin{bmatrix} T_1^{n+1} \\ . \\ . \\ . \\ T_{M-1}^{n+1} \\ q_1^{n+1} \\ T_{M+1}^{n+1} \\ . \\ . \\ . \\ T_{N-1}^{n+1} \end{bmatrix} \tag{B.2}$$

The matrix $\underline{T}^n$ of equation (2.12) is:

$$\underline{T}^n = \begin{bmatrix} T_1^n \\ . \\ . \\ . \\ T_{M-1}^n + \lambda T_M^{n+1} \\ T_M^n - (2\lambda + 1) T_M^{n+1} \\ T_{M+1}^n + \lambda T_M^{n+1} \\ . \\ . \\ . \\ {T_{N-1}}^n + \lambda {T_N}^{n+1} \end{bmatrix} \tag{B.3}$$

Because at measurement position $x = \chi_M$, temperature ${T_M}^{n+1}$ is known, by applying the left hand side unknown boundary condition ${q_1}^{n+1}$, we can substitute ${q_1}^{n+1}$ (the heat flux of the left boundary $x = 0$ as shown in figure B.1) into the

left side matrix $\underline{T}^{n+1}$. Then the unknowns of the matrix $\underline{T}^{n+1}$ can be solved by the time-marching scheme.

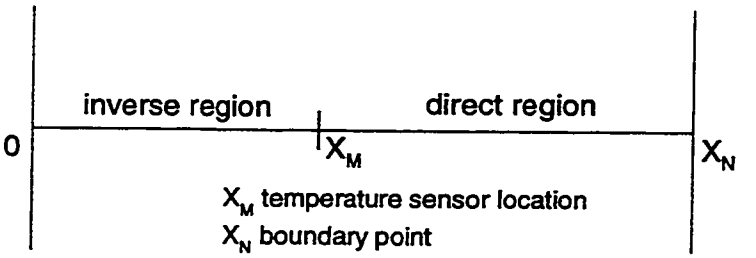

Unknown conditions:
$Q(0,t) = ?$
$T(0,t) = ?$

Known conditions:
$T(X_N,t)$ = Known temperature at X_N
$T(X_M,t)$ = Known temperature at X_M

Figure B.1: One-dimensional inverse heat conduction problem: model II

Appendix C

Derivation of Right and Left Hand Inversion Boundary Conditions in Chapter 2

Derive equations (2.16) and (2.17) as follows:

The dimensionless one-dimensional heat equation is:

$$\frac{\partial T}{\partial t} = \frac{\partial^2 T}{\partial x^2} \tag{C.1}$$

Apply heat flux q at the right hand boundary and discretize the heat equation into an implicit finite difference form. Then apply the unknown boundary temperature (T_N^{n+1}) and heat flux (q_N^{n+1}) at the right hand side as follows:

$$\frac{\partial T}{\partial t} = \frac{\partial q}{\partial x} \tag{C.2}$$

where q is heat flux. Then

$$\frac{T_N^{n+1} - T_N^n}{\Delta t} = \frac{1}{\Delta x}\left[q_N^{n+1} - \frac{T_N^{n+1} - T_{N-1}^{n+1}}{\Delta x}\right] \tag{C.3}$$

$$\left(1 + \frac{\Delta t}{(\Delta x)^2}\right) T_N^{n+1} - \frac{\Delta t}{(\Delta x)^2} T_{N-1}^{n+1} - \frac{\Delta t}{\Delta x} q_N^{n+1} = T_N^n \tag{C.4}$$

Similarly the left hand boundary is:

$$\left(1 + \frac{\Delta t}{(\Delta x)^2}\right) T_o^{n+1} - \frac{\Delta t}{(\Delta x)^2} T_1^{n+1} + \frac{\Delta t}{\Delta x} q_o^{n+1} = T_o^n \tag{C.5}$$

It can be seen that the coefficients q_o^{n+1} and q_n^{n+1} are $+\frac{\Delta t}{\Delta x}$ and $-\frac{\Delta t}{\Delta x}$, respectively.

Appendix D

Derivation of Equations (3.3) to (3.11)

Derive equations (3.3)-(3.11) as follows:

Assume the second order differential equation has the following form:

$$\frac{d^2T}{dt^2} + c_1\frac{dT}{dt} + c_2T = a(t) \tag{D.1}$$

where T is the temperature variable, t is the time, $a(t)$ is the external temperature "force" function, c_1 and c_2 are constants. We may rearrange equation (D.1) by letting

$$T = z_1 \tag{D.2}$$

and

$$\frac{dT}{dt} = z_2 \tag{D.3}$$

rewrite equation (D.3)

$$\frac{dz_1}{dt} = z_2 \tag{D.4}$$

then equation (D.1) can be represented as follows

$$\frac{dz_2}{dt} = -c_2 z_1 - c_1 z_2 + a(t) \tag{D.5}$$

In matrix notation, equations (D.4) and (D.5) become:

$$\begin{bmatrix} \frac{dz_1}{dt} \\ \frac{dz_2}{dt} \end{bmatrix} = \begin{bmatrix} 0 & 1 \\ -c_2 & -c_1 \end{bmatrix} \begin{bmatrix} z_1 \\ z_2 \end{bmatrix} + \begin{bmatrix} 0 \\ 1 \end{bmatrix} a(t) \tag{D.6}$$

For example, assume $c_1 = 0$ and $c_2 = 0$, we have

$$\begin{bmatrix} \frac{dz_1}{dt} \\ \frac{dz_2}{dt} \end{bmatrix} = \begin{bmatrix} 0 & 1 \\ 0 & 0 \end{bmatrix} \begin{bmatrix} z_1 \\ z_2 \end{bmatrix} + \begin{bmatrix} 0 \\ 1 \end{bmatrix} a(t) \tag{D.7}$$

This is the matrix form of equation (3.7) in Chapter 3. Then, we integrate the following two equations with respect to time variable from t to τ

$$\frac{dz_1}{dt} = z_2 \tag{D.8}$$

$$\frac{dz_2}{dt} = a(t) \tag{D.9}$$

to obtain

$$z_1(t) = z_1(\tau) + (t-\tau)z_2(t) + \frac{a(t)}{2}(t-\tau)^2 \tag{D.10}$$

$$z_2(t) = z_2(\tau) + a(t)(t-\tau) \tag{D.11}$$

Equations (D.10)-(D.11) are equations (3.10)-(3.11) in the Chapter 3.